INSTITUTE OF PHYSICS PUBLISHING INVERSE PROBLEMS

Inverse Problems **21** (2005) 1715–1744 doi:10.1088/0266-5611/21/5/013

Migration/inversion: think image point coordinates, process in acquisition surface coordinates

Norman Bleistein[1], **Yu Zhang**[2], **Sheng Xu**[2], **Guanquan Zhang**[3] **and Samuel H Gray**[4]

[1] Center for Wave Phenomena, Department of Geophysics, Colorado School of Mines, Golden, CO 80401-1887, USA
[2] Veritas DGC Inc., 10300 Town Park Drive, Houston, TX 77072, USA
[3] Institute of Computational Mathematics and Sci/Eng Computing, Academy of Mathematics and System Sciences, Chinese Academy of Sciences, Beijing, 100080, People's Republic of China
[4] Veritas DGC Inc., 715 Fifth Avenue SW, Suite 2200 Calgary, Alberta, T2P 5A2, Canada

Received 12 April 2005
Published 16 September 2005
Online at stacks.iop.org/IP/21/1715

Abstract

We state a general principle for seismic migration/inversion (M/I) processes: think image point coordinates; compute in surface coordinates. This principle allows the natural separation of multiple travel paths of energy from a source to a reflector to a receiver. Further, the Beylkin determinant (Jacobian of transformation between processing parameters and acquisition surface coordinates) is particularly simple in stark contrast to the common-offset Beylkin determinant in standard single arrival Kirchhoff M/I.

A feature of this type of processing is that it changes the deconvolution structure of Kirchhoff M/I operators or the deconvolution imaging operator of wave equation migration into convolution operators; that is, division by Green's functions is replaced by multiplications by adjoint Green's functions.

This transformation from image point coordinates to surface coordinates is also applied to a recently developed extension of the standard Kirchhoff inversion method. The standard method uses WKBJ Green's functions in the integration process and tends to produce more imaging artefacts than alternatives, such as methods using Gaussian beam representations of Green's functions in the inversion formula. These methods point to the need for a true-amplitude Kirchhoff technique that uses more general Green's functions: Gaussian beams, true-amplitude one-way Green's functions, or Green's functions from the two-way wave equation. Here, we present a derivation of a true-amplitude Kirchhoff M/I that uses these more general Green's functions. When this inversion is recast as an integral over all sources and receivers, the formula is surprisingly simple.

1. Introduction

Xu *et al* (2001) presented a two-dimensional (2D) Kirchhoff inversion formula as an integral of input reflection data over all possible dip angles at an image point for each fixed value of the opening (or scattering) angle between the rays from the source and receiver at an image point. They then recast the result as an integral over source and receiver points on the acquisition surface. Bleistein and Gray (2002) presented a three-dimensional (3D) version of that formula. The transformation between image point coordinates and surface coordinates involves ray Jacobians for the rays from the image point to the source and receiver point.

More recently, in a true-amplitude wave equation migration (WEM), Zhang *et al* (2004a) introduced an extra integration in the processing formula. This additional integration computes the average of outputs over a small patch of opening and azimuth angles at the image point. Each angle pair at the image point corresponds to a different source point at the upper surface. Thus, integrating over an angular patch on the unit sphere of directions at the image point is equivalent to integrating over the output from a collection over outputs from a set of WEMs. Of course, such a transformation of coordinates has a Jacobian that arises in a standard manner in the computation. That Jacobian is closely related to the ray Jacobian associated with the amplitude propagation from the source point to the image point. These authors went a step further, however, and rewrote the Jacobian in terms of the ray-theoretic amplitude to which it is related. As a consequence, the deconvolution imaging condition of WEM was transformed into a correlation imaging condition for true-amplitude WEM. The correlation-type imaging condition is attractive because it does not involve division by the amplitude of a Green's function.

There is clearly a paradox: the integral kernel of the original WEM imaging condition is a quotient of solutions of the wave equation and the modified WEM imaging condition is a product of solutions, both leading to a true-amplitude implementation of WEM. This paradox will be resolved through the derivation of the correlation form of the imaging condition. Note that we have shown in an earlier paper (Zhang *et al* 2003) that the deconvolution form of the imaging condition as modified by our theory, will produce the same peak amplitude as Kirchhoff inversion, when the wavefields in the formula are replaced by their ray-theoretic approximations. Since the transformation to the convolution form is achieved by an exact change of variables, there is no further analysis required to predict that the peak amplitude of the convolution imaging condition produces a true-amplitude result in the same sense.

This observation that we can transform a deconvolution-type imaging formula into a correlation-type imaging formula has motivated a re-examination of recently derived results for Kirchhoff M/I; namely, to derive similar correlation-type processes for Kirchhoff imaging and inversion processes. This leads to Kirchhoff M/I formulae as sums over sources and receivers at the upper surface, while retaining two important features of the formulae for integration over image point angular coordinates: (i) multi-pathing of rays is fully accounted for in all but a few pathological cases and (ii) the Beylkin determinant is easy to calculate. (This determinant is the Jacobian of transformation between processing parameters and acquisition surface coordinates.) This last observation is most important when one considers the difficulties in computing the Beylkin determinant for common-offset M/I in 3D.

Separately, Bleistein (2003) proposed a method for extending Kirchhoff M/I to M/Is with other than ray-theoretic Green's functions. (We present this derivation in an appendix to this paper since it has only appeared previously in an internal report.) Green's functions in this

M/I are fairly arbitrary; they could be Gaussian beams or true-amplitude one-way[5] Green's functions or full waveform Green's functions derived from the two-way wave equation. Each improvement in Green's function type will produce a corresponding improvement in the quality of the image while retaining the same level of amplitude fidelity of the original multi-arrival Kirchhoff inversion. No matter what choice of Green's function is used here, we still need specific ray-theoretic information, namely, the WKBJ Green's function amplitudes and the Beylkin determinant. These arise from asymptotically calculating a normalization factor of the final Kirchhoff inversion with the chosen Green's functions. If we did not use this approximation, then we would need to carry out a pointwise sixfold integration for the purposes of normalization of the amplitude of the kernel.

An important concept about true-amplitude processing is at work here. 'True-amplitude' as applied to the output of an inversion algorithm refers to estimation of plane-wave reflection coefficients. For anything but plane-wave reflection from planar reflectors in a homogeneous medium, this is a WKBJ-approximate estimate and has little or no meaning in the context of full waveform solutions of the wave equation. Thus, although we image better with better Green's functions, reflection coefficients are estimated via ray-theoretic asymptotic solutions. Hence, the normalization factors need to be no better than what is provided by ray theory, while the general Green's functions used in the extended algorithm are expected to be numerically close to the WKBJ Green's function when they are evaluated away from caustics and other anomalies. Thus, we contend that there is both heuristic and physical justification for this simplification.

This full waveform Kirchhoff inversion also benefits from starting with a formula that is an integration over angular variables at the image point and transforming to source/receiver coordinates. When this is done, the WKBJ normalization is no longer explicit in the inversion formula. Ray theory is used in this final result only to sort the output into panels defined by common opening angle/common azimuth angle (COA/CAA) of the rays at the image point.

To summarize, if we start with a Kirchhoff M/I in migration dip coordinates, the transformation to surface coordinates can be applied. As in the more classical Kirchhoff M/I, this will produce an output that is separated into COA/CAA gathers. The result of that transformation on this Kirchhoff M/I with more general Green's functions is described here, as well.

Kirchhoff inversion of data gathered from parallel lines of multi-streamer data is both particularly important and particularly elusive. In 3D, the classical Kirchhoff inversion applies to data sets defined by two spatial parameters that characterize the source/receiver distribution. So, for example, one might think of common-offset data in which the two parameters define the midpoint between the source and receiver at a fixed azimuth (compass direction) on the acquisition surface, or one might think of common-shot data in which the source point is fixed and the two parameters describe the receiver location. Each shot of a multi-streamer survey 'looks like' a common-shot data set, except that the data acquisition in the orthogonal direction to the streamer set is too narrow for common-shot M/I. Thus, it is necessary to use data from all of the shots to generate an inversion output. Consequently, we must work with a four spatial parameter data set: two parameters for each source location and two parameters for each receiver location. Thus, the Kirchhoff inversion that we present here, as an integral over all sources and receivers, provides such an inversion. We are not aware of any other Kirchhoff inversion that applies to this type of data acquisition.

[5] These are full waveform solutions of the one-way wave equation having the property that their WKBJ approximations agree asymptotically with the WKBJ approximations for the full wave equation. In that sense they are 'true-amplitude one-way' Green's functions.

We present results in the order of progressing complexity. We begin with a discussion of the recent result for true-amplitude WEM where a summation over the angle (in 2D) or angle pair (in 3D) is transformed to summation over acquisition surface source coordinate(s). We then consider Kirchhoff inversion in image point coordinates and describe the transformation to source and receiver coordinates. Finally, we discuss the extension of Kirchhoff inversion to employ more general Green's functions for improved image quality while maintaining the true-amplitude character of Kirchhoff inversion.

For this paper, 'true amplitude' has a specific and limited meaning. First, it is a model-consistent estimate of a plane-wave reflection coefficient at an incidence angle determined by the specular incident and reflected rays. Second, it is an asymptotic estimate of that plane-wave reflection coefficient within an aperture that is limited by the acquisition geometry, again determined by the rays. As regards the latter, it is necessary for some neighbourhood, say, a Fresnel zone, around the specular ray to lie in the aperture of arrivals at the receiver array (e.g., Hertweck *et al* (2003)). When these conditions are met, extensive evidence through synthetic tests suggests that the 'true amplitude' of the theory is accurately estimated.

Certain technical issues concern the validity of the transformations between angular coordinates at depth and acquisition surface coordinates. These issues can be dealt with by separating the transformation domain into a union of domains where the transformation is single valued in each of the sub-domains.

2. Estimating the reflection coefficient as an average over opening angles in true-amplitude WEM

Here, we describe the process of averaging true-amplitude WEM outputs over image point angle(s) and then transforming this average to a sum over source points. Zhang *et al* (2004a, 2004b) described a theory for determining true-amplitude solutions to one-way wave equations for upward and downward propagating waves. In the context of forward modelling, 'true amplitude' means that the wavefunctions agree asymptotically with ray-theoretical solutions outside of the vicinity where the ray Jacobian is zero.

Using Claerbout's (1970) one-way wave equations as a point of departure, the new one-way wave equations require an additional term to modulate the amplitude, and a modification of the source for the downgoing wave. These governing equations are given by equations (31) and (32) in Zhang *et al* (2003). The specifics of this method are not of interest here. Suffice it to say that it leads to true-amplitude waveforms $p_D(\boldsymbol{x}_s, \boldsymbol{x}, \omega)$ and $p_U(\boldsymbol{x}_r, \boldsymbol{x}_s, \boldsymbol{x}, \omega)$, the former being the downgoing field in response to the physical source and the latter being the upward propagating wave that provides the observed data at the receiver array on the acquisition surface.

More important for the discussion here is the imaging condition for these solutions:

$$R(\boldsymbol{x}, \theta) = \frac{1}{2\pi} \int \frac{p_U(\boldsymbol{x}_r, \boldsymbol{x}_s, \boldsymbol{x}, \omega)}{p_D(\boldsymbol{x}_s, \boldsymbol{x}, \omega)} \, \mathrm{d}\omega. \tag{1}$$

In this equation, the incidence angle θ can be a multi-valued function of $\boldsymbol{x}_s$, but $\boldsymbol{x}_s$ is a single-valued function of θ. This is the incidence angle of the specular ray from the source measured from the normal to the reflector at the image point; see figure 1. By tracing a ray from the source to the image point and estimating the dip direction at the image point, the specular value of θ can be estimated.

The waves used here are different from those used in Claerbout's (1971, 1985) deconvolution imaging condition. Zhang *et al* (2003) have shown that equation (1) reduces to the Kirchhoff inversion formula for common-shot data given by Bleistein *et al* (2001). In turn,

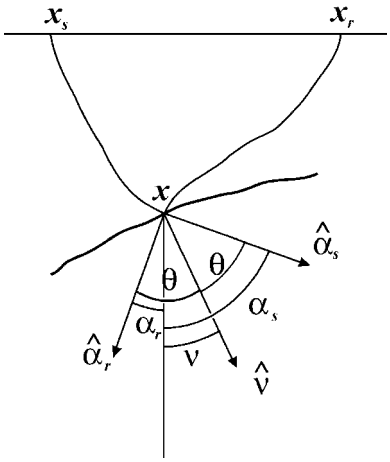

Figure 1. Coordinates of the 2D inversion process. $\boldsymbol{x}$: the image point. $\boldsymbol{x}_s$ and $\boldsymbol{x}_r$: the source and specular receiver, respectively. θ: the incident specular angle of the source ray, also the reflection angle with respect to the normal. $\hat{\boldsymbol{\alpha}}_s$ and $\hat{\boldsymbol{\alpha}}_r$: unit vectors along the specular rays from the image point to the source and receiver, respectively. $\hat{\boldsymbol{\nu}}$: migration dip; also at specular, unit normal to the reflector. α_s, α_r, ν: angles with respect to the vertical of the vectors $\hat{\boldsymbol{\alpha}}_s, \hat{\boldsymbol{\alpha}}_r, \hat{\boldsymbol{\nu}}$.

this reference contains a proof that the output has a peak value on the reflector proportional to an angularly dependent reflection coefficient (angle θ) at the specular angle (for which Snell's law is satisfied by the ray directions at the image point).

Remark. Briefly, the connection with common-shot Kirchhoff inversion goes as follows. The observed data at the upper surface, $p_U(\boldsymbol{x}_r, \boldsymbol{x}_s, \boldsymbol{x}, \omega)$, can be back-projected into the subsurface by using Green's theorem. The result is

$$p_U(\boldsymbol{x}_r, \boldsymbol{x}_s, \boldsymbol{x}, \omega) = 2\mathrm{i}\omega \int \frac{\cos\beta_r'}{v(\boldsymbol{x}_r')} p_U(\boldsymbol{x}_r, \boldsymbol{x}_s, \boldsymbol{x}_r', \omega) A(\boldsymbol{x}_r', \boldsymbol{x}) \exp\{-\mathrm{i}\omega\tau(\boldsymbol{x}_r', \boldsymbol{x})\}\, \mathrm{d}\boldsymbol{x}_r'. \tag{2}$$

Here, β_r' is the dip angle of the ray from $\boldsymbol{x}$ to $\boldsymbol{x}_r'$.

When this representation is substituted into equation (1) the result is

$$R(\boldsymbol{x}, \theta) = \frac{1}{\pi} \int \mathrm{i}\omega \frac{\cos\beta_r'}{v(\boldsymbol{x}_r')} \frac{A(\boldsymbol{x}_r', \boldsymbol{x})}{p_D(\boldsymbol{x}_s, \boldsymbol{x}, \omega)} p_U(\boldsymbol{x}_r, \boldsymbol{x}_s, \boldsymbol{x}_r', \omega) \exp\{-\mathrm{i}\omega\tau(\boldsymbol{x}_r', \boldsymbol{x})\}\, \mathrm{d}\omega\, \mathrm{d}\boldsymbol{x}_r'. \tag{3}$$

Next, we replace p_D by its ray-theoretic approximation, namely,

$$p_D(\boldsymbol{x}_s, \boldsymbol{x}, \omega) \sim A(\boldsymbol{x}, \boldsymbol{x}_s) \exp\{-\mathrm{i}\omega\tau(\boldsymbol{x}, \boldsymbol{x}_s)\} \tag{4}$$

to obtain the common-shot Kirchhoff inversion formula

$$R(\boldsymbol{x}, \theta) = \frac{1}{\pi} \int \mathrm{i}\omega \frac{\cos\beta_r'}{v(\boldsymbol{x}_r')} \frac{A(\boldsymbol{x}_r', \boldsymbol{x})}{A(\boldsymbol{x}, \boldsymbol{x}_s)} p_U(\boldsymbol{x}_r, \boldsymbol{x}_s, \boldsymbol{x}_r', \omega) \cdot \exp\{-\mathrm{i}\omega[\tau(\boldsymbol{x}_r', \boldsymbol{x}) + \tau(\boldsymbol{x}, \boldsymbol{x}_s)]\}\, \mathrm{d}\omega\, \mathrm{d}\boldsymbol{x}_r', \tag{5}$$

which is the true-amplitude common-shot inversion formula as proposed by Keho and Beydoun (1988) and by Hanitzsch (1997).

This result disregards phase shifts at caustics in the downward propagation of the two wavefields. As will be seen below, this is a minor omission for which the correction is straightforward.

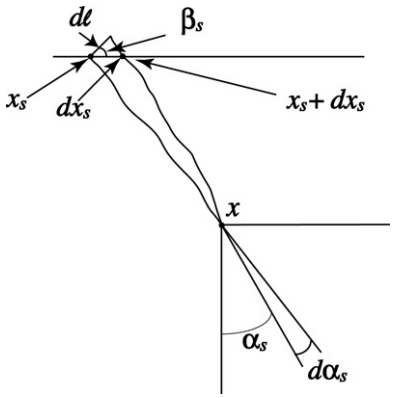

Figure 2. Relationship between α_s and $\boldsymbol{x}_s$ defined by rays. The width of the ray tube $\mathrm{d}\ell$ is related to $\mathrm{d}x_s$, the horizontal variation along the acquisition surface, through the cosine of the dip angle of the ray with respect to the normal (not shown). This angle is the same as the angle between $\mathrm{d}\ell$ and $\mathrm{d}x_s$.

In the application, we have to contend with the issue of discretization in the estimate of $R(\boldsymbol{x}, \theta)$. We expect that noise due to discretization and truncation can be attenuated by averaging over nearby values of incidence angle around the given incidence angle, all at the same image point. Therefore we propose to average over a set of angles near a particular incidence angle θ. Varying the incidence angle at the image point is equivalent—via a mapping by rays—to varying the source point at the upper surface; that is, varying the incidence angle is equivalent to varying the shot and data set to which the WEM is applied. Thus, we consider the imaging condition

$$\overline{R(\boldsymbol{x}, \theta)} = \frac{1}{2\pi\,\Delta\theta} \int \mathrm{d}\omega \int_{\theta-\Delta\theta/2}^{\theta+\Delta\theta/2} \frac{p_U(\boldsymbol{x}_r, \boldsymbol{x}_s, \boldsymbol{x}, \omega)}{p_D(\boldsymbol{x}_s, \boldsymbol{x}, \omega)}\, \mathrm{d}\theta', \tag{6}$$

where $\overline{R(\boldsymbol{x}, \theta)}$ denotes an average, in general; here, over the angle θ'.

In figure 1, the choice of $\hat{\boldsymbol{\nu}}$ that represents the *geological dip angle* is fixed for a given image point. Then we can see that θ and α_s differ by a constant angle, namely, this reflector dip angle: $\theta = \alpha_s - \nu$. Thus, for this fixed $\hat{\boldsymbol{\nu}}$, integrating over θ is equivalent to integrating over α_s. Further, varying α_s leads to variations in $\boldsymbol{x}_s$ that are defined via the propagation of rays from the image point $\boldsymbol{x}$ to the source point $\boldsymbol{x}_s$. Pictorially, we can see the relationship in figure 2. The width of the ray tube $\mathrm{d}\ell$ is related to $\mathrm{d}x_s$, the horizontal variation of source location along the acquisition surface, through the cosine of the angle that the ray direction makes with the vertical. This angle is the same as the angle between $\mathrm{d}\ell$ and $\mathrm{d}x_s$. Of course, the differential cross section of the ray tube is related to $\mathrm{d}\alpha_s$ through the ray Jacobian, which, in turn, is related to the 2D WKBJ Green's function amplitude.

The mathematical details of this discussion are carried out in appendix A. The bottom line is that, in equation (6),

$$\mathrm{d}\theta' = 8\pi\, A(\boldsymbol{x}_s, \boldsymbol{x}) A^*(\boldsymbol{x}_s, \boldsymbol{x}) \frac{\cos\beta_s}{v(\boldsymbol{x}_s)}\, \mathrm{d}x_s, \tag{7}$$

where * denotes the complex conjugate.

We remark that the interval $(\theta - \Delta\theta/2, \theta + \Delta\theta/2)$, centred at θ, does not map into a symmetric interval in sources about the central source $x_s(\theta)$. Below, we will denote the interval in source coordinates by $(x_s - \Delta_-, x_s + \Delta_+)$.

By using $\mathrm{d}\theta'$ as defined in equation (7) in the reflectivity-averaging equation (6), we find that

$$\overline{R(\boldsymbol{x},\theta)} = \frac{4}{\Delta\theta}\int \mathrm{d}\omega \int_{x_s-\Delta_-}^{x_s+\Delta_+} A(\boldsymbol{x}'_s,\boldsymbol{x})A^*(\boldsymbol{x}'_s,\boldsymbol{x})\frac{\cos\beta'_s}{v(\boldsymbol{x}'_s)}\frac{p_U(\boldsymbol{x}_r,\boldsymbol{x}'_s,\boldsymbol{x},\omega)}{p_D(\boldsymbol{x}'_s,\boldsymbol{x},\omega)}\,\mathrm{d}x'_s. \tag{8}$$

In this equation, θ on the left-hand side and $\boldsymbol{x}_s$ in the limits of integration on the right-hand side are connected by the ray that propagates from the image point to $\boldsymbol{x}_s$.

Recall that the concept of 'true amplitude' makes sense only when the image is produced by a single arrival and certain asymptotic approximations are valid. One of those approximations is

$$A(\boldsymbol{x}_s,\boldsymbol{x})A^*(\boldsymbol{x}_s,\boldsymbol{x}) \approx p_D(\boldsymbol{x}_s,\boldsymbol{x},\omega)p_D^*(\boldsymbol{x}_s,\boldsymbol{x},\omega). \tag{9}$$

Using this approximation in the averaged reflectivity of equation (8) yields

$$\overline{R(\boldsymbol{x},\theta)} = \frac{4}{\Delta\theta}\int \mathrm{d}\omega \int_{x_s-\Delta_-}^{x_s+\Delta_+} \frac{\cos\beta'_s}{v(\boldsymbol{x}'_s)}p_D^*(\boldsymbol{x}'_s,\boldsymbol{x},\omega)p_U(\boldsymbol{x}_r,\boldsymbol{x}'_s,\boldsymbol{x},\omega)\,\mathrm{d}x'_s. \tag{10}$$

Comparing the right-hand side here with the right-hand side of the reflectivity definition, equation (1), we see that a deconvolution-type imaging formula has been recast as a correlation-type imaging formula by averaging over incidence angles at the image point and then transforming that angular integral into an integral over source locations at the upper surface. As noted in the introduction, we are assured that the correlation form of the imaging condition in equation (10) is true amplitude in our sense of that term.

Suppose that we were to follow the same line of reasoning on the imaging formula of equation (10) that led to the common-shot inversion formula of equation (5). We would find exactly the same travel time appearing in the phase of the resulting asymptotic approximation to the right-hand side of equation (10). Thus, we can expect that the same reflector map will arise from the processing suggested by the averaged imaging condition defined by equation (10).

Furthermore, apart from the averaging, we applied exact or leading-order asymptotic substitutions to equation (1) to obtain the imaging condition of equation (10). At worst, then, we anticipate that the peak output of equation (10) would differ from the peak output of the original imaging condition in equation (1) by the effect of averaging over a small range of nearby outputs arising from different source gathers.

We remark that whether we compute the averaged reflectivity from equation (6), which is an integral over dip angle, or from equation (10), which is an integral over sources, it is necessary to compute ray trajectories from the upper surface to the image point. Equation (10) would seem to require a further calculation of an image interval $(x_s - \Delta_-, x_s + \Delta_+)$ from the interval $(\theta - \Delta\theta/2, \theta + \Delta\theta/2)$.

As an alternative, we propose the following procedure to compute the averages over all θ intervals. Decompose the θ domain into intervals of length $\Delta\theta$. For each input trace—that is, for each source/receiver pair—determine the angle θ' and the angle β'_s. Calculate the integrand and add it to a running sum in the appropriate θ interval. For sufficiently small $\Delta\theta$, even if there is multi-pathing, the separate trajectories from the source to image point will produce values of θ that are separated by more than the width $\Delta\theta$ that defines the bin size. This method accumulates the average reflectivity for all θ intervals simultaneously.

We note further that the first representation of the averaged reflectivity, equation (6), has an alternative interpretation. It is the discrete form of the seemingly redundant distributional equation

$$R(\boldsymbol{x},\theta) = \frac{1}{2\pi}\int \mathrm{d}\omega \int \frac{p_U(\boldsymbol{x}_r,\boldsymbol{x}_s,\boldsymbol{x},\omega)}{p_D(\boldsymbol{x}_s,\boldsymbol{x},\omega)}\delta(\theta-\theta')\,\mathrm{d}\theta'. \tag{11}$$

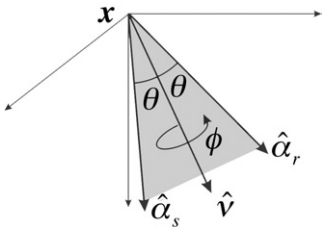

Figure 3. Migration/inversion image point coordinates in 3D. All unit vectors are now functions of two angles. $\hat{\boldsymbol{\nu}}$, $\hat{\boldsymbol{\alpha}}_s$ and $\hat{\boldsymbol{\alpha}}_r$ all lie in the same plane. Further, there are two angles, θ and ϕ, to characterize the positions of the unit vectors from the source and receiver with respect to the migration dip vector, $\hat{\boldsymbol{\nu}}$.

In transforming from this result back to the discrete form of the averaged reflectivity in equation (6), $\Delta\theta$ is the 'weight' of the discrete approximation to the delta-function and the integral yields an estimate of the distributional integral over the interval of length $\Delta\theta$.

Whether we proceed from the average reflectivity of equation (6) or the distributional reflectivity of equation (11), we still arrive at equation (10)—the average reflectivity as a sum over sources and receivers—by transforming from image point coordinates to acquisition surface coordinates.

2.1. Three dimensions

The 3D version of this result is somewhat more complicated to derive. The relevant coordinates at the image point $\boldsymbol{x}$ are shown in figure 3. The unit vectors are now functions of two angles. Further, there are two angles, θ and ϕ, characterizing the relationship of the unit vectors from the source and receiver, $\hat{\boldsymbol{\alpha}}_s$ and $\hat{\boldsymbol{\alpha}}_r$, respectively, to the dip vector $\hat{\boldsymbol{\nu}}$.

The averaging process must now be an integration over θ and ϕ, with differential element $\sin\theta'\,\mathrm{d}\theta'\,\mathrm{d}\phi'$; that is,

$$\overline{R(\boldsymbol{x},\theta,\phi)} = \frac{1}{2\pi|\Omega|}\int \mathrm{d}\omega \int_{\Omega} \frac{p_U(\boldsymbol{x}_r,\boldsymbol{x}_s,\boldsymbol{x},\omega)}{p_D(\boldsymbol{x}_s,\boldsymbol{x},\omega)}\sin\theta'\,\mathrm{d}\theta'\,\mathrm{d}\phi'. \tag{12}$$

In this equation, Ω represents an angular domain in θ' and ϕ' centred is around θ and ϕ. We use $|\Omega|$ as the area of this domain, equivalently, the differential area element on the unit sphere covered by varying θ and ϕ.

We now need to transform from the two variables θ' and ϕ' to the two variables x_{s1} and x_{s2}. The Jacobian of this transformation is derived in appendix B. From that discussion, we find that

$$\sin\theta'\,\mathrm{d}\theta'\,\mathrm{d}\phi' = 16\pi^2 v(\boldsymbol{x})A(\boldsymbol{x}_s,\boldsymbol{x})A^*(\boldsymbol{x}_s,\boldsymbol{x})\frac{\cos\beta'_{s1}}{v(\boldsymbol{x}_s)}\,\mathrm{d}x_{s1}\,\mathrm{d}x_{s2}. \tag{13}$$

Here, β'_s is the angle between the ray direction (or the normal to the ray tube cross section) and the normal to the differential source area cross section. Equation (13) should be compared with the differential $\mathrm{d}\theta'$, equation (7), which is the appropriate angular differential in 2D. Substituting the expression for the differential angular area element of equation (13) into the averaged reflectivity result, equation (12), leads to

$$\overline{R(\boldsymbol{x},\theta,\phi)} = \frac{8\pi}{|\Omega|}\int \mathrm{d}\omega \int_{\Delta} v(\boldsymbol{x})p_D^*(\boldsymbol{x}_s,\boldsymbol{x},\omega)p_U(\boldsymbol{x}_r,\boldsymbol{x}_s,\boldsymbol{x},\omega)\frac{\cos\beta'_{s1}}{v(\boldsymbol{x}_s)}\,\mathrm{d}x_{s1}\,\mathrm{d}x_{s2}. \tag{14}$$

In this equation, Δ is the image on the acquisition surface of the angle domain Ω in θ' and ϕ'. Again, this correlation-type imaging condition is a true amplitude in the sense that we define that term.

As in 2D, we do not propose determining the domain Δ in equation (14). Instead, we discretize the angular domain on the unit sphere of directions defined by θ and ϕ. For each source/receiver pair, we accumulate the integrand into running sums in the appropriate θ, ϕ sub-domain as discussed above for the 2D case.

The 3D averaged reflectivity defined by equation (12) has a distributional interpretation similar to the equivalence between the 2D reflectivity average, equation (6), and its distributional equivalent, equation (11). The correct identity arises from the observation that

$$1 = \frac{1}{|\Omega|}\int_\Omega \sin\theta'\,\mathrm{d}\theta'\,\mathrm{d}\phi' = \int_\Omega \delta(\theta-\theta')\delta(\sin\theta'(\phi-\phi'))\sin\theta'\,\mathrm{d}\theta'\,\mathrm{d}\phi'$$
$$= \int_\Omega \delta(\theta-\theta')\delta(\phi-\phi')\,\mathrm{d}\theta'\,\mathrm{d}\phi'. \tag{15}$$

Here, $\mathrm{d}\theta'$ and $\sin\theta'\,\mathrm{d}\phi'$ are differential arc length variables in the polar and azimuthal directions, respectively; hence, the second equality. The third equality then follows from the distributional identity succinctly stated as $|a|\delta(ax) = \delta(x)$. In this case, the reflectivity average defined by equation (12) is a discretization of the distributional form of the reflectivity expressed in either of the following two forms:

$$R(\boldsymbol{x},\theta,\phi) = \frac{1}{2\pi}\int \mathrm{d}\omega \int_\Omega \frac{p_U(\boldsymbol{x}_r,\boldsymbol{x}_s,\boldsymbol{x},\omega)}{p_D(\boldsymbol{x}_s,\boldsymbol{x},\omega)}\delta(\theta-\theta')\delta(\sin\theta'(\phi-\phi'))\sin\theta'\,\mathrm{d}\theta'\,\mathrm{d}\phi'$$
$$= \frac{1}{2\pi}\int \mathrm{d}\omega \int_\Omega \frac{p_U(\boldsymbol{x}_r,\boldsymbol{x}_s,\boldsymbol{x},\omega)}{p_D(\boldsymbol{x}_s,\boldsymbol{x},\omega)}\delta(\theta-\theta')\delta(\phi-\phi')\,\mathrm{d}\theta'\,\mathrm{d}\phi'. \tag{16}$$

As before, these seemingly redundant identities allow us to transform between integrals in image domain angular coordinates and integrals in surface coordinates by proceeding with the change of variables described above.

2.2. *Observations*

The pattern of the discussion here will be repeated in the following sections. The objective is to transform integrals in image point angular variables to acquisition surface variables. The change of variables can be decomposed into three main factors—derivatives or Jacobians—through application of the chain rule for differentiation. The factors are listed here:

(i) The first factor arises from a change of variables from the original angle(s) of the integration to the angle(s) of the ray direction vector(s). (In the example of this section, only the direction of the ray from the source to the image point was of interest.)

(ii) The next transformation involves the ray Jacobian(s): to transform a differential element in direction angles to a differential element of the ray tube cross section. It is this factor that is rewritten in terms of WKBJ Green's function amplitudes.

(iii) The last factor arises from a projection of the ray tube cross section onto the acquisition surface. In the discussions in this paper, we assume that the acquisition surface is flat. However, the transformation is only slightly more complicated when the acquisition surface is curved. For example, we would replace the variables x_{s1}, x_{s2} by two parameters, say σ_{s1}, σ_{s2} with the surface described by a vector function $(\boldsymbol{x}_s(\sigma_{s1},\sigma_{s2}))$. Then, we would make the replacement

$$\mathrm{d}x_{s1}\,\mathrm{d}x_{s2} \quad \Rightarrow \quad \left|\frac{\partial \boldsymbol{x}_s}{\partial\sigma_{s1}} \times \frac{\partial \boldsymbol{x}_s}{\partial\sigma_{s2}}\right| \mathrm{d}\sigma_{s1}\,\mathrm{d}\sigma_{s2}$$

for the differential element in the average reflectivity in equation (14). Furthermore, β_s now becomes the angle between the normal to this differential surface element and the normal to the differential cross section of the ray tube—equivalently, the ray direction. Of course, the same idea would apply to integrals over receivers in the discussions below. We will not refer to this extension any further as we proceed to address Kirchhoff M/I.

In the current example, the first factor in this list was equal to unity in 2D and was equal to a ratio of trigonometric factors in 3D. The second factor is the ray Jacobian for rays from the image point to the source point. The third factor is simply the cosine of the ray dip angle at the acquisition surface, with only an additional scaling as noted immediately above, if the acquisition surface is not a plane.

In each case here, and below, the correlation-type processing formulae produce a true-amplitude output in the same sense as the classical Kirchhoff inversion of Bleistein *et al* (2001). In contrast to the deconvolution formulae of that text, these formulae do not require division by ray-theoretic (or WKBJ) amplitudes that become progressively smaller with increasing depth into the subsurface.

3. 3D Kirchhoff M/I with summation over migration dip angles

We now turn to Kirchhoff M/I and show how these same ideas allow us to transform inversion formulae written as integrals in angular variables at an image point to integrals over all traces on the acquisition surface.

Bleistein and Gray (2002) derived M/I as an integration over the directions of the migration dip directions of the unit vector $\hat{\boldsymbol{\nu}}$ in figure 3. The integral was then transformed into one over the source and receiver coordinates on the acquisition surface. That result was stated in terms of the ray Jacobians that transform the angular coordinates of $\hat{\boldsymbol{\alpha}}_s$ and $\hat{\boldsymbol{\alpha}}_r$ of figure 3 to the source and receiver coordinates, respectively. Here we go one step further, expressing those Jacobians in terms of the 3D WKBJ amplitudes of the ray-theoretic Green's functions connecting the image point with the source and receiver point, respectively.

Our starting point is equation (26) of Bleistein and Gray. However, that result was equivalent to the reflectivity β of Bleistein *et al* (2001), equation (5.1.21). Here we prefer to use the equivalent of β_1 (not to be confused with the dip angle β_s of figure 2), given by equation (5.1.47) in the same reference, but rewritten in terms of the variables of this paper.

Remark. The reflectivity function β yields a reflectivity map whose peak value on a reflector is

$$\beta^{\text{peak}} = R(\boldsymbol{x}, \theta, \phi)\frac{\cos\theta}{2\pi\, v(\boldsymbol{x})}\int F(\omega)\,\mathrm{d}\omega.$$

In this equation, R is the geometrical optics or plane-wave reflection coefficient at the specular reflection angles θ and ϕ, $v(\boldsymbol{x})$ is the wave speed, and $F(\omega)$ is the source signature. On the other hand, β_1 yields a reflectivity map whose peak value on the reflector is

$$\beta_1^{\text{peak}} = R(\boldsymbol{x}, \theta, \phi)\frac{1}{2\pi}\int F(\omega)\,\mathrm{d}\omega.$$

The reflectivity β is a scaled band limited delta-function in space with dimension 1/LENGTH, while β_1 is a scaled band limited delta-function in time with dimension 1/TIME, both under the assumption that the source signature given by $F(\omega)$ is dimensionless. Both functions are scaled by the geometrical optics reflection coefficient but they differ by a factor of $\cos\theta/v(\boldsymbol{x})$. Thus, the quotient provides an estimate of the cosine of the specular reflection angle. Parenthetically (off the subject of this paper), in tests of numerical accuracy of this method, our experience

is that the percentage error in the estimates of $\cos\theta$ is typically an order of magnitude smaller than the error in the estimate of the reflection coefficient itself. We explain this by the fact that the integrands for these two reflectivity operators differ by only one factor and we expect that their errors will trend in the same direction. Consequently, when we examine the quotient that produces the estimate of $\cos\theta/v(\boldsymbol{x})$, the form of this quotient is

$$\frac{\cos\theta}{v(\boldsymbol{x})}\cdot\frac{1+\epsilon_1}{1+\epsilon_2}\approx\frac{\cos\theta}{v(\boldsymbol{x})}\cdot[1+\epsilon_1-\epsilon_2+\cdots],$$

with ϵ_1 and ϵ_2 *having the same sign*; that is, the fractional error in the quotient turns out to be approximately the magnitude of the difference of the fractional errors of the two separate integrals and thereby smaller in magnitude than either of the separate errors.

Rewritten in terms of the variables of this paper, the reflectivity β_1 is

$$\mathcal{R}(\boldsymbol{x},\theta,\phi)=\frac{1}{4\pi^2}\frac{2\cos\theta}{v(\boldsymbol{x})}\int\frac{D_3(\boldsymbol{x},\boldsymbol{x}_r,\boldsymbol{x}_s)}{A(\boldsymbol{x},\boldsymbol{x}_s)A(\boldsymbol{x},\boldsymbol{x}_r)}\sin\nu_1\,\mathrm{d}\nu_1\,\mathrm{d}\nu_2. \tag{17}$$

Here, D_3 is a filtered version of the input traces:

$$D_3(\boldsymbol{x},\boldsymbol{x}_r,\boldsymbol{x}_s)=\frac{1}{2\pi}\int \mathrm{i}\omega u(\boldsymbol{x}_r,\boldsymbol{x}_s,\omega)\cdot\exp(-\mathrm{i}\omega\tau(\boldsymbol{x},\boldsymbol{x}_s,\boldsymbol{x}_r)+\mathrm{i}K(\boldsymbol{x},\hat{\boldsymbol{\nu}},\theta,\phi)\mathsf{sgn}(\omega)\pi/2)\,\mathrm{d}\omega. \tag{18}$$

In this equation, $u(\boldsymbol{x}_r,\boldsymbol{x}_s,\omega)$ is the observed data on the input trace with source $\boldsymbol{x}_s$ and receiver $\boldsymbol{x}_r$; $K(\boldsymbol{x},\hat{\boldsymbol{\nu}},\theta,\phi)$ is the KMAH index of the ray trajectory from the source to the image point $\boldsymbol{x}$ to the receiver. The KMAH index is a count of phase shifts due to caustics that the rays pass through on the total trajectory (Chapman 1985, Kravtsov and Orlov 1993).

The formula in equation (17) is an integral over two variables to be carried out for each fixed value of the opening angle θ and the azimuthal angle ϕ of figure 3. The output then is a suite of reflectivity functions where each one is a panel for fixed values of these angles.

Our objective is to recast this result as an integral over the source and receiver points. However, each of those is a function of two parameters so that the final integral will be over four variables, while the integral in equation (17) is over only two variables. In the simplest case, the four variables of integration in the new formula are just the horizontal components of the source and receiver points, respectively, but they could be other parameters describing an arbitrary acquisition surface. If we could transform the representation of reflectivity, equation (17), as an integral over polar coordinates at the image point into an integral over the coordinates of $\hat{\boldsymbol{\alpha}}_s$ and $\hat{\boldsymbol{\alpha}}_r$, then we would be able to follow the method of the previous section and appendix B to recast the result as an integral over source and receiver coordinates. Of course, these latter two unit vectors are themselves each a function of two variables—four altogether—while the right-hand side of equation (17) is an integration over only two angles. The first trick, then, is to rewrite the right-hand side as an integral in the four variables, ν_1, ν_2, θ and ϕ. This leads to a representation that echoes the distributional form of the averaged reflectivity, equation (16), of the previous section. The result of rewriting the reflectivity of equation (17) as an integral in four variables was stated earlier in equation (35) in Bleistein and Gray (2002):

$$\begin{aligned}\mathcal{R}(\boldsymbol{x},\theta,\phi)&=\frac{1}{4\pi^2}\int\frac{2\cos\theta'}{v(\boldsymbol{x})}\frac{D_3(\boldsymbol{x},\boldsymbol{x}_r,\boldsymbol{x}_s)}{A(\boldsymbol{x},\boldsymbol{x}_s)A(\boldsymbol{x},\boldsymbol{x}_r)}\delta(\theta'-\theta)\delta(\phi'-\phi)\sin\nu_1\,\mathrm{d}\nu_1\,\mathrm{d}\nu_2\,\mathrm{d}\theta'\,\mathrm{d}\phi'\\&=\frac{1}{4\pi^2}\int\frac{2\cos\theta'}{v(\boldsymbol{x})}\frac{D_3(\boldsymbol{x},\boldsymbol{x}_r,\boldsymbol{x}_s)}{A(\boldsymbol{x},\boldsymbol{x}_s)A(\boldsymbol{x},\boldsymbol{x}_r)}\delta(\theta'-\theta)\delta(\sin\theta'(\phi'-\phi))\\&\qquad\cdot\sin\nu_1\,\mathrm{d}\nu_1\,\mathrm{d}\nu_2\sin\theta'\,\mathrm{d}\theta'\,\mathrm{d}\phi'.\end{aligned} \tag{19}$$

Here, the Dirac delta-functions provide a device by which the integral in two variables is recast as an integral in four variables. In the second form, the argument of each delta-function can be viewed as an arc length along the two orthogonal angular coordinates on the unit sphere of directions of travel time gradient at the image point; see equation (15), which relates the discrete average over a patch on the unit sphere to a distributional integral over the same patch.

We have now prepared the inversion formula for transformation to source and receiver variables. As described in the outline at the end of the previous section, this transformation is done in stages. With reference to the variables depicted in figure 3, we first transform from $\nu_1, \nu_2, \theta', \phi'$ to $\alpha_{s1}, \alpha_{s2}, \alpha_{r1}, \alpha_{r2}$ and then transform these variables to surface variables through ray Jacobians. This derivation is carried out in appendix C. Using the result (C.5) from the appendix in the representation (19) for the reflectivity as an integral over four angles at the image point leads to

$$\mathcal{R}(\boldsymbol{x}, \theta, \phi) = 32\pi^2 v(\boldsymbol{x}) \int \frac{\cos\beta_s}{v(\boldsymbol{x}_s)} \frac{\cos\beta_r}{v(\boldsymbol{x}_r)} D_3(\boldsymbol{x}, \boldsymbol{x}_r, \boldsymbol{x}_s) A^*(\boldsymbol{x}_s, \boldsymbol{x}) A^*(\boldsymbol{x}_r, \boldsymbol{x}) \cdot \delta(\theta' - \theta)\delta(\sin\theta'(\phi' - \phi))\, \mathrm{d}x_{s1}\, \mathrm{d}x_{s2}\, \mathrm{d}x_{r1}\, \mathrm{d}x_{r2}. \tag{20}$$

In this equation, as in the previous section, θ', ϕ', β_s and β_r are all functions of the integration variables defined through the changes of variables. In the computation, these angles are measured by ray tracing from the source and receiver point to the image point. Thus, there is no need to define them explicitly in terms of the integration variables.

In practice, this integral will be carried out discretely. To do so, we replace each of the delta-functions with a discrete approximation and then restrict the domain of integration to cover the support of the discrete delta-functions (domain of nonzero values of the discrete delta-functions). Therefore, let us set

$$\delta(\theta - \theta') \approx \begin{cases} \dfrac{1}{\Delta\theta}, & \theta - \Delta\theta/2 \leqslant \theta' \leqslant \theta + \Delta\theta/2, \\ 0, & \text{otherwise.} \end{cases}$$

$$\delta(\sin\theta'(\phi - \phi')) \approx \begin{cases} \dfrac{1}{\sin\theta'\Delta\phi}, & \phi - \Delta\phi/2 \leqslant \phi' \leqslant \phi + \Delta\phi/2, \\ 0, & \text{otherwise.} \end{cases}$$

The dual range $(\theta - \Delta\theta/2, \theta + \Delta\theta/2, \phi - \Delta\phi/2, \phi + \Delta\phi/2)$ defines a domain on the unit sphere, Ω, with area $|\Omega| = \sin\theta\Delta\theta\Delta\phi$. We denote the image of Ω under the mapping by rays to the upper surface as the range Δ. Then the discrete version of equation (20) for the reflectivity function as an integral over all sources and receivers is

$$\overline{\mathcal{R}(\boldsymbol{x}, \theta, \phi)} = \frac{32\pi^2 v(\boldsymbol{x})}{|\Omega|} \int_\Delta \frac{\cos\beta_{s1}}{v(\boldsymbol{x}_s)} \frac{\cos\beta_{r1}}{v(\boldsymbol{x}_r)} D_3(\boldsymbol{x}, \boldsymbol{x}_r, \boldsymbol{x}_s) \cdot A^*(\boldsymbol{x}_s, \boldsymbol{x}) A^*(\boldsymbol{x}_r, \boldsymbol{x})\, \mathrm{d}x_{s1}\, \mathrm{d}x_{s2}\, \mathrm{d}x_{r1}\, \mathrm{d}x_{r2}. \tag{21}$$

Here, we are justified introducing the overbar $\overline{\mathcal{R}}$ because the result again has the form of an average.

The average reflectivity of equation (21) should be compared with that of equation (14), the average over sources for the reflectivity generated by true-amplitude WEM. In the former result, the integration is over sources, while in the latter $p_U(\boldsymbol{x}_r, \boldsymbol{x}_s, \boldsymbol{x}, \omega)$ is the back-projection of the observed data. Thus, we could think of $p_U(\boldsymbol{x}_r, \boldsymbol{x}_s, \boldsymbol{x}, \omega)$ as being prescribed by a convolution of the observed data with a Green's function, hence, an integral over receivers for each fixed source point. In this regard, both are integrals over all sources and receivers. One common feature of these reflectivity formulae, equations (21) and (14), is their dimensionality; that is, if

we assume that the wavefields have dimension of 1/LENGTH, then both of these reflectivities have the dimension of 1/TIME. For the Kirchhoff result in the above equation, (21), we know that this is the correct dimensionality (of the function β_1 of the Kirchhoff inversion theory).

However, the derivations of equations (14) and (21) are quite different. Further, as noted, the integrand in equation (21) involves three wavefields, namely, the two WKBJ Green's functions and the observed data, through D_3, while the formula in equation (14) requires two. Equation (14) is derived as an average over sources—that is, an average over experiments—while the reflectivity of equation (21) is derived from an arbitrary and unspecified data acquisition geometry later summed over a secondary set of angles. In other words, we use a double coverage of directions defined on the unit sphere at the image point to produce this inversion formula (21). The symmetry in this formula is apparent: WKBJ Green's function amplitudes, dip angles at the source and receiver points, and wave speeds at those points play an equal role in the final formula. In our experience, this type of symmetric, universal formula is elusive if one begins from common-shot or common-offset Kirchhoff inversion. The main point that is missed in common-shot or common-offset inversion is the sorting in the opening and azimuth angle of the ray pairs at the image point.

One application of the average reflectivity defined by equation (21) achieves an inversion in COA/CAA panels where such an inversion cannot be derived from standard Kirchhoff inversion: namely, inversion of swath data, where an array of parallel receiver streamers all receive data from each shot. However, each swath is narrow. There is insufficient azimuthal coverage on the upper surface for each shot to derive a reliable 3D inversion. Furthermore, there is no acquisition surface Kirchhoff method available to provide an image from all shots. This acquisition surface coverage requires using data from all sources and receivers to achieve a 3D migration or inversion. The reflectivity formulae here, equations (20) and (21), provide exactly the M/I processing needed for this type of data acquisition. This process will provide adequate coverage in θ although its coverage in ϕ is limited.

In summary, starting from a Kirchhoff M/I formula as an integral in migration dip direction coordinates at an image point, we have derived a Kirchhoff M/I as an integral over all sources and receivers at the upper surface; that is, over all data traces. The formula is not limited by acquisition geometry, but the reliability of the output certainly is: we create an image and a reliable estimate of the reflection coefficient only for those patches on the unit sphere of dip directions which lie with the illumination domain of the rays, usually defined by the Fresnel zone.

4. Full waveform Kirchhoff-approximate modelling and inversion

We change directions at this point to describe an extension of Kirchhoff modelling and inversion using full waveform Green's functions. We remind the reader that for us 'true amplitude' is meant in an asymptotic (ray-theoretic) sense. In forward modelling, this means that the wavefield is well approximated by one or a sum of WKBJ contributions, with travel time determined by the eikonal equation, amplitude determined by the transport equation, and with a possible additional phase shift adjustments provided by the KMAH index.

For inversion, we have already described 'true amplitude' to mean an output that has the peak value proportional to the WKBJ plane-wave reflection coefficient. This is predicted by the theory only when the image is generated by a single specular ray trajectory from the source to image point to receiver. When there are multiple arrivals, the image is created by an overlay of contributions from specular source/receiver pairs with different reflection coefficients. At

such points, it is not important what the weighting is, except that it has the right order of magnitude for balancing with the output from other image points.

After deriving the full waveform Kirchhoff inversion formula, we will specialize it to inversion in migration dip angles, thereby connecting this new result to the theory presented in the earlier sections.

The basic steps in the method are as follows:

(1) Start from the Kirchhoff approximation as a volume integral, but use any form of Green's function, as suggested above. In this form of the Kirchhoff approximation, the reflectivity function appears explicitly under the integral sign and the output is (synthetic) model data for any source/receiver pair.
(2) View this representation as a modelling operator operating on the reflectivity function. Write down a pseudo-inverse operator on the data to obtain an inversion for the reflectivity.
(3) Use asymptotics to simplify the operator, but preserve the more general Green's functions where possible so as not to destroy the central character of the degree of imaging quality of the inversion.

4.1. Kirchhoff modelling

The forward modelling Kirchhoff approximation is derived in appendix D. The new feature here is that the result uses full waveform Green's functions. For example, we could use Green's functions generated by Gaussian beams, solutions of true-amplitude one-way wave equations or solutions of the two-way wave equation. Furthermore, we write the Kirchhoff approximation as a *volume* integral, rather than a surface integral. This is now fairly standard when the forward model is used in inversion theory.

The upward reflected wavefield from a source $\boldsymbol{x}_s$ measured at a receiver $\boldsymbol{x}_r$ is

$$u_R(\boldsymbol{x}_r, \boldsymbol{x}_s, \omega) \sim -\mathrm{i}\omega F(\omega) \int_S \mathcal{R}_0(\boldsymbol{x}', \theta, \phi) |\nabla_{x'}\phi| G_s(\boldsymbol{x}', \boldsymbol{x}_s, \omega) G_r(\boldsymbol{x}_r, \boldsymbol{x}', \omega)\, \mathrm{d}V. \tag{22}$$

In this equation $\mathcal{R}_0(\boldsymbol{x}, \theta, \phi)$ is what we mean by the *reflectivity* function denoted by $\beta(\boldsymbol{x}') = R(\boldsymbol{x}', \theta, \phi)\gamma(\boldsymbol{x}')$ in Bleistein *et al* (2001). Here, use of the notation $\mathcal{R}_0(\boldsymbol{x}, \theta, \phi)$ is consistent with using $\mathcal{R}(\boldsymbol{x}, \theta, \phi)$ for β_1 of that reference. The function $\gamma(\boldsymbol{x}')$ is the *singular function* of the reflection surface as defined in that reference. This is a delta-function of normal distance to the surface. The scale factor R is the geometrical optics reflection coefficient at incident angle θ; we also allow for an azimuthal dependence ϕ.

It is this representation that we propose to invert for $\mathcal{R}_0$ and then modify to obtain a formula for $\mathcal{R}$.

4.2. The inversion process

Here, we describe the inversion process for the data representation given in equation (22). Let us suppose that we have some two-parameter set of sources and receivers on the acquisition surface. Bleistein *et al* (2001) denote those two parameters by $\boldsymbol{\xi} = (\xi_1, \xi_2)$. Such a parametrization allows us to describe common-shot, common-offset or common-scattering-angle source/receiver pairs, among others. However, there is no reason to be specific at this time. The data, then, are a function of three variables, $\boldsymbol{\xi}$ and ω.

For the moment, we introduce a shorthand notation for the representation of equation (22), namely,

$$u_R \sim K[\mathcal{R}_0], \tag{23}$$

suggesting the idea that the observed field is produced by an operator K operating on the reflectivity $\mathcal{R}_0$. Symbolically, we want to obtain an approximate inversion of this equation by applying a pseudo-inverse operator to the data; that is,

$$\mathcal{R}_0 = \|(K^\dagger K)^{-1}\| K^\dagger [u_R]. \tag{24}$$

Here, $K^\dagger$ is the adjoint operator to the operator K. The cascade of operators, $K^\dagger K$, is called the normal operator; $\|(K^\dagger K)^{-1}\|$ is appropriate normalization intended to produce an asymptotic 'true-amplitude' inverse in the output. Further, the source signature $F(\omega)$ is a part of u_R, yielding, at best, a band limited inversion in frequency. There are also aperture limitations on this result; we cannot produce $\mathcal{R}_0$ where the reflector is not illuminated by the source(s) with reflection data observed at the receiver(s). With all of these caveats, we still expect that, in some band limited and aperture limited sense, $\|(K^\dagger K)^{-1}\| K^\dagger K$ acts as a delta-function in the spatial variables, namely, $\|(K^\dagger K)^{-1}\| K^\dagger K \approx \delta(\boldsymbol{x} - \boldsymbol{x}')$.

To apply this operator, we need to carry out an integration in the variables $\boldsymbol{\xi}$ and ω with an appropriate integration kernel. Just as the kernel K had two sets of arguments, $\boldsymbol{x}'$ and $\boldsymbol{\xi}$, ω, the kernel of this pseudo-inverse has two sets of arguments, now $\boldsymbol{x}$ and $\boldsymbol{\xi}$, ω. Thus, the symbolic inversion in equation (24) actually produces $\mathcal{R}_0(\boldsymbol{x}, \theta, \phi)$.

The pseudo-inversion applied to equation(22) is

$$\mathcal{R}_0(\boldsymbol{x}, \theta, \phi) = \int \mathrm{i}\omega \|(K^\dagger K)^{-1}\| |\nabla_x \phi(\boldsymbol{x}, \boldsymbol{\xi})| G_s^*(\boldsymbol{x}_s, \boldsymbol{x}, \omega) G_r^*(\boldsymbol{x}, \boldsymbol{x}_r, \omega) u_R(\boldsymbol{x}_r, \boldsymbol{x}_s, \omega)\, \mathrm{d}^2\xi\, \mathrm{d}\omega. \tag{25}$$

In this equation,

$$\|(K^\dagger K)^{-1}\| = \left| \int \mathrm{d}^2\xi \omega^2\, \mathrm{d}\omega \int \mathrm{d}V |\nabla_x \phi(\boldsymbol{x}, \boldsymbol{\xi})| G_s^*(\boldsymbol{x}_s, \boldsymbol{x}, \omega) G_r^*(\boldsymbol{x}, \boldsymbol{x}_r, \omega) \right.$$
$$\left. \cdot |\nabla_y \phi(\boldsymbol{x}', \boldsymbol{\xi})| G_s(\boldsymbol{x}', \boldsymbol{x}_s, \omega) G_r(\boldsymbol{x}_r, \boldsymbol{x}', \omega) \right|^{-1}, \tag{26}$$

with

$$\tau(\boldsymbol{x}, \boldsymbol{\xi}) = \tau(\boldsymbol{x}, \boldsymbol{x}_s) + \tau(\boldsymbol{x}, \boldsymbol{x}_r), \qquad \tau(\boldsymbol{x}', \boldsymbol{\xi}) = \tau(\boldsymbol{x}', \boldsymbol{x}_s) + \tau(\boldsymbol{x}', \boldsymbol{x}_r). \tag{27}$$

4.3. Analysis of the pseudo-inverse norm $\|(K^\dagger K)^{-1}\|$

Clearly, we do not want to carry out the sixfold integral of the norm indicated in the definition (26). Fortunately, it is not necessary to do so. As noted above, accurate 'amplitude' in standard Kirchhoff inversion has relevance only when the image is created by a single arrival. Therefore we might as well replace this norm by its asymptotic expansion under the assumption that there is only a single arrival. This is accomplished by using ray theory to approximate Green's functions in the integrand of equation (26) that defines the norm $\|(K^\dagger K)^{-1}\|$: all of the more accurate Green's functions have the same ray-theoretic approximation, consistent with the underlying full wave equation. This is an important principle that is fundamental to extracting amplitude information from inversion processes with more general Green's functions than those provided by WKBJ.

Asymptotic analysis of this norm then leads to a calculation almost identical to that used to derive the Kirchhoff inversion in the first place. The details are carried out in appendix E. The final result is

$$\|(K^\dagger K)^{-1}\| = \frac{1}{8\pi^3} \frac{|h(\boldsymbol{x}, \boldsymbol{\xi})|}{|\nabla_x \tau(\boldsymbol{x}, \boldsymbol{\xi})|^2} \frac{1}{|A_s(\boldsymbol{x}, \boldsymbol{x}_s) A_r(\boldsymbol{x}_r, \boldsymbol{x})|^2}. \tag{28}$$

In this equation, $h(\boldsymbol{x}, \boldsymbol{\xi})$ is the Beylkin determinant defined by equation (E.4).

4.4. Full waveform Kirchhoff inversion

Next, we use the approximation in equation (28) in the representation (25) for $\mathcal{R}_0(\boldsymbol{x}, \theta, \phi)$ to obtain

$$\mathcal{R}_0(\boldsymbol{x}, \theta, \phi) = \frac{1}{8\pi^3} \int \frac{G_s^*(\boldsymbol{x}_s, \boldsymbol{x}, \omega) G_r^*(\boldsymbol{x}, \boldsymbol{x}_r, \omega)}{|A_s(\boldsymbol{x}, \boldsymbol{x}_s) A_r(\boldsymbol{x}_r, \boldsymbol{x})|^2} \frac{|h(\boldsymbol{x}, \boldsymbol{\xi})|}{|\nabla_x \tau(\boldsymbol{x}, \boldsymbol{\xi})|} \mathrm{i}\omega u_R(\boldsymbol{x}_r, \boldsymbol{x}_s, \omega)\, \mathrm{d}\omega\, \mathrm{d}^2\xi. \quad (29)$$

When the Green's functions here are replaced by their ray-theoretic approximations, this formula reduces to the general inversion formula for β in Bleistein *et al* (2001), equation (5.1.21). This assures us that the reflectivity function produces the reflection coefficient times the band limited singular function of the reflector (with dimension 1/LENGTH) when the image is produced by a single arrival. As in earlier sections, we prefer to work with a reflectivity that is the equivalent of β_1 with dimension 1/TIME. We will see below that the final integrand for this latter reflectivity is slightly easier to calculate. The only difference between the integrands of these two reflectivities is an additional factor of $|\nabla_x \tau(\boldsymbol{x}, \boldsymbol{\xi})|$ in the denominator of the integrand for β_1; that is,

$$\mathcal{R}(\boldsymbol{x}, \theta, \phi) = \frac{1}{8\pi^3} \int \frac{G_s^*(\boldsymbol{x}_s, \boldsymbol{x}, \omega) G_r^*(\boldsymbol{x}, \boldsymbol{x}_r, \omega)}{|A_s(\boldsymbol{x}, \boldsymbol{x}_s) A_r(\boldsymbol{x}_r, \boldsymbol{x})|^2} \frac{|h(\boldsymbol{x}, \boldsymbol{\xi})|}{|\nabla_x \tau(\boldsymbol{x}, \boldsymbol{\xi})|^2} \mathrm{i}\omega u_R(\boldsymbol{x}_r, \boldsymbol{x}_s, \omega)\, \mathrm{d}\omega\, \mathrm{d}^2\xi. \quad (30)$$

Next, we use the result

$$\frac{|h(\boldsymbol{x}, \boldsymbol{\xi})|}{|\nabla_x \tau(\boldsymbol{x}, \boldsymbol{\xi})|^2} = \left[\frac{2\cos\theta}{v(\boldsymbol{x})}\right] \left|\frac{\partial \hat{\boldsymbol{\nu}}}{\partial \xi_1} \times \frac{\partial \hat{\boldsymbol{\nu}}}{\partial \xi_2}\right| \quad (31)$$

derived in appendix F. Then equation (30) becomes

$$\mathcal{R}(\boldsymbol{x}, \theta, \phi) = \frac{1}{8\pi^3} \int \frac{G_s^*(\boldsymbol{x}_s, \boldsymbol{x}, \omega) G_r^*(\boldsymbol{x}, \boldsymbol{x}_r, \omega)}{|A_s(\boldsymbol{x}, \boldsymbol{x}_s) A_r(\boldsymbol{x}_r, \boldsymbol{x})|^2} \left[\frac{2\cos\theta}{v(\boldsymbol{x})}\right] \cdot \left|\frac{\partial \hat{\boldsymbol{\nu}}}{\partial \xi_1} \times \frac{\partial \hat{\boldsymbol{\nu}}}{\partial \xi_2}\right| \mathrm{i}\omega u_R(\boldsymbol{x}_r, \boldsymbol{x}_s, \omega)\, \mathrm{d}\omega\, \mathrm{d}^2\xi. \quad (32)$$

Equation (32) can also be expressed totally in terms of full waveform Green's functions by observing that to leading order asymptotically,

$$|A_s(\boldsymbol{x}, \boldsymbol{x}_s) A_r(\boldsymbol{x}_r, \boldsymbol{x})|^2 \sim |G_s(\boldsymbol{x}, \boldsymbol{x}_s, \omega) G_r(\boldsymbol{x}_r, \boldsymbol{x}, \omega)|^2 . \quad (33)$$

In this case, the reflectivity representation in equation (32) becomes

$$\mathcal{R}(\boldsymbol{x}, \theta, \phi) = \frac{1}{8\pi^3} \int \frac{1}{G_s(\boldsymbol{x}_s, \boldsymbol{x}, \omega) G_r(\boldsymbol{x}, \boldsymbol{x}_r, \omega)} \left[\frac{2\cos\theta}{v(\boldsymbol{x})}\right] \cdot \left|\frac{\partial \hat{\boldsymbol{\nu}}}{\partial \xi_1} \times \frac{\partial \hat{\boldsymbol{\nu}}}{\partial \xi_2}\right| \mathrm{i}\omega u_R(\boldsymbol{x}_r, \boldsymbol{x}_s, \omega)\, \mathrm{d}\omega\, \mathrm{d}^2\xi. \quad (34)$$

We remark that

$$\left|\frac{\partial \hat{\boldsymbol{\nu}}}{\partial \xi_1} \times \frac{\partial \hat{\boldsymbol{\nu}}}{\partial \xi_2}\right| \mathrm{d}^2\xi$$

is the differential cross-sectional area on the unit sphere of migration dip directions $\hat{\boldsymbol{\nu}}$, traced out as ξ_1, ξ_2 vary. Traditionally, these variables might be the midpoint and azimuth of a multi-azimuth common-offset survey, or the receiver coordinates in a common-source survey. We see here, then, that even when these variables represent coordinates on the acquisition surface, true-amplitude processing cannot avoid a computational connection between those coordinates and the migration dip coordinates. Indeed, in the case of common offset/common azimuth, direct computation of the cross product is impractical.

Equation (34) is a full waveform Kirchhoff inversion of deconvolution type. We have not been explicit here about the coordinates ξ_1, ξ_2 because there is no need to do so. Thus, this formula applies whether we use surface coordinates, such as midpoints in a common-offset/common-azimuth survey, or image point coordinates such as the polar angles of the migration dip vector $\hat{\boldsymbol{\nu}}$.

4.5. Full waveform inversion in migration angular coordinates recast as an integral in source/receiver coordinates

We are now prepared to connect full waveform Kirchhoff inversion to the theme of the earlier sections of the paper. As a first step, we specialize the last two representations of the reflectivity to the case where ξ_1 and ξ_2 are just the polar angles ν_1 and ν_2 used in the earlier sections of the paper. In this case, one can check that

$$\left| \frac{\partial \hat{\boldsymbol{\nu}}}{\partial \xi_1} \times \frac{\partial \hat{\boldsymbol{\nu}}}{\partial \xi_2} \right| = \left| \frac{\partial \hat{\boldsymbol{\nu}}}{\partial \nu_1} \times \frac{\partial \hat{\boldsymbol{\nu}}}{\partial \nu_2} \right| = \sin \nu_1. \tag{35}$$

Now, the reflectivity as defined by equations (32) and (34) become

$$\mathcal{R}(\boldsymbol{x}, \theta, \phi) = \frac{1}{8\pi^3} \int \frac{G_s^*(\boldsymbol{x}_s, \boldsymbol{x}, \omega) G_r^*(\boldsymbol{x}, \boldsymbol{x}_r, \omega)}{|A_s(\boldsymbol{x}, \boldsymbol{x}_s) A_r(\boldsymbol{x}_r, \boldsymbol{x})|^2} \cdot \left[\frac{2 \cos \theta}{v(\boldsymbol{x})} \right] \mathrm{i}\omega u_R(\boldsymbol{x}_r, \boldsymbol{x}_s, \omega) \, \mathrm{d}\omega \sin \nu_1 \, \mathrm{d}\nu_1 \, \mathrm{d}\nu_2, \tag{36}$$

and

$$\mathcal{R}(\boldsymbol{x}, \theta, \phi) = \frac{1}{8\pi^3} \int \frac{1}{G_s(\boldsymbol{x}_s, \boldsymbol{x}, \omega) G_r(\boldsymbol{x}, \boldsymbol{x}_r, \omega)} \cdot \left[\frac{2 \cos \theta}{v(\boldsymbol{x})} \right] \mathrm{i}\omega u_R(\boldsymbol{x}_r, \boldsymbol{x}_s, \omega) \, \mathrm{d}\omega \sin \nu_1 \, \mathrm{d}\nu_1 \, \mathrm{d}\nu_2, \tag{37}$$

respectively.

Equation (36) should be compared to the Kirchhoff inversion (17) derived using WKBJ Green's functions, observing that in equation (17)

$$\frac{1}{|A_s(\boldsymbol{x}, \boldsymbol{x}_s) A_r(\boldsymbol{x}_r, \boldsymbol{x})|^2} \sin \nu_1 \, \mathrm{d}\nu_1 \, \mathrm{d}\nu_2 = \frac{1}{A_s^*(\boldsymbol{x}, \boldsymbol{x}_s) A_r^*(\boldsymbol{x}_r, \boldsymbol{x})} \frac{1}{A_s(\boldsymbol{x}, \boldsymbol{x}_s) A_r(\boldsymbol{x}_r, \boldsymbol{x})} \sin \nu_1 \, \mathrm{d}\nu_1 \, \mathrm{d}\nu_2.$$

Equation (17) was recast as an integral over source/receiver coordinates in equation (20). In that process, the factors

$$\frac{1}{4\pi^2} \frac{2 \cos \theta}{v(\boldsymbol{x})} \frac{1}{A(\boldsymbol{x}, \boldsymbol{x}_s) A(\boldsymbol{x}, \boldsymbol{x}_r)} \sin \nu_1 \, \mathrm{d}\nu_1 \, \mathrm{d}\nu_2$$

were replaced by

$$16\pi \frac{\cos \beta_{s1}}{v(\boldsymbol{x}_s)} \frac{\cos \beta_{r1}}{v(\boldsymbol{x}_r)} \frac{v(\boldsymbol{x})}{\sin \theta'} A^*(\boldsymbol{x}_s, \boldsymbol{x}) A^*(\boldsymbol{x}_r, \boldsymbol{x}) \delta(\theta' - \theta) \delta(\phi' - \phi) \, \mathrm{d}x_{s1} \, \mathrm{d}x_{s2} \, \mathrm{d}x_{r1} \, \mathrm{d}x_{r2}.$$

Thus, we can recast the full waveform reflectivity in equation (36) as an integral over source/receiver coordinates by making the same replacements in this reflectivity formula; that is,

$$\mathcal{R}(\boldsymbol{x}, \theta, \phi) = 16\pi v(\boldsymbol{x}) \int G_s^*(\boldsymbol{x}_s, \boldsymbol{x}, \omega) G_r^*(\boldsymbol{x}, \boldsymbol{x}_r, \omega) \mathrm{i}\omega u_R(\boldsymbol{x}_r, \boldsymbol{x}_s, \omega) \, \mathrm{d}\omega \cdot \frac{\cos \beta_s}{v(\boldsymbol{x}_s)} \frac{\cos \beta_r}{v(\boldsymbol{x}_r)} \delta(\theta' - \theta) \delta(\sin \theta' (\phi' - \phi)) \, \mathrm{d}x_{s1} \, \mathrm{d}x_{s2} \, \mathrm{d}x_{r1} \, \mathrm{d}x_{r2}. \tag{38}$$

This inversion formula for reflectivity should be compared to the Kirchhoff inversion formula (20) which uses the ray-theoretic Green's function. In that equation, the Fourier transform of the filtered data is carried out in advance. The travel time in that result became the phase of the Fourier transform and the amplitudes of the WKBJ Green's functions are only a function of the spatial variables. Here, the dependence of Green's functions on frequency is more complicated, so the frequency domain integral is no longer a simple Fourier transform. We can no longer pre-process the data by Fourier transform and simply evaluate it at the travel time. The entire integrand must be computed for each ω and then integrated over that variable.

On the other hand, the reflectivity of equation (38) is a full waveform generalization of Kirchhoff inversion, written as a sum over all sources and receivers. The delta-functions here separate the output into COA/CAA panels ready for AVA analysis.

With the reflectivity of equation (20) that used WKBJ Green's functions, we went one step further by discretizing the delta-functions, essentially producing an averaging-type reflectivity function in equation (21). The analogous result here is

$$\overline{\mathcal{R}(\boldsymbol{x},\theta,\phi)} = \frac{16\pi}{|\Omega|}\int_{\Delta} G_s^*(\boldsymbol{x}_s,\boldsymbol{x},\omega)G_r^*(\boldsymbol{x},\boldsymbol{x}_r,\omega)\mathrm{i}\omega u_R(\boldsymbol{x}_r,\boldsymbol{x}_s,\omega)\,\mathrm{d}\omega \cdot \frac{\cos\beta_{s1}}{v(\boldsymbol{x}_s)}\frac{\cos\beta_{r1}}{v(\boldsymbol{x}_r)}\,\mathrm{d}x_{s1}\,\mathrm{d}x_{s2}\,\mathrm{d}x_{r1}\,\mathrm{d}x_{r2}. \tag{39}$$

All of the discussion about computation of the reflectivity (20) with a distributional integrand, and equation (21), with continuous integrand, applies here as well. We see here that the computation of a full waveform true-amplitude Kirchhoff inversion is a fairly simple expression: the essential elements are the two Green's functions, the filter $i\omega$, the observed data, and dip-correction factors at the source and receiver points. However, since we do not use WKBJ Green's functions, the usual Fourier transform pre-processing of the data cannot be carried out.

Let us summarize what was done in this section:

(1) We started from a forward model of reflection data as a volume integral, using the Kirchhoff approximation to represent the reflected wave on the reflector in terms of the incident wave and the geometrical optics reflection coefficient.
(2) We then introduced a pseudo-inverse of this modelling operator to produce an inversion formula for the reflectivity in terms of the observed data at the acquisition surface.
(3) This pseudo-inverse required calculation of the integral norm of the normal operator, which is the cascade of the modelling operator with its formal adjoint. This was calculated asymptotically using WKBJ approximations of Green's functions appearing in this sixfold integral.
(4) The general inversion formula that resulted was then specialized to using the image point migration dip polar angles as the variables of integration and recasting the result as an integral over sources and receivers.

This process led to equation (39) for full waveform reflectivity as an integral over all sources and receivers resulting in an output in COA/CAA panels. This is a correlation-type inversion formula.

Use of the full waveform Green's functions in the Kirchhoff approximation and then use of their WKBJ approximations in the estimate of the magnitude of the normal operator both depend on the basis of 'true-amplitude' Kirchhoff inversion. Our ultimate objective as regards amplitude is an estimate of the non-normal incidence plane-wave reflection coefficient at each point on the reflector. This coefficient is generalized via ray theory from plane waves incident on planar reflectors in homogeneous media to curved wave fronts incident on curved

reflectors in heterogeneous media. As such, the concept only has meaning when we can speak of single arrivals at the reflector in media whose length scales allow the WKBJ waveform to make sense. Thus, the interchange between full waveform Green's functions and their WKBJ approximations wherever amplitude issues are concerned also makes sense; we do no better at reflection amplitude estimates when we use the full waveform Green's functions than when we use their WKBJ approximations. However, the full waveform Green's functions do provide better image quality.

5. Summary and conclusions

We have considered three approaches to migration/inversion, namely WEM, traditional Kirchhoff migration and an extension of the Kirchhoff method to full waveform imaging. In the first case, integration of image point angle(s) was introduced as an averaging process. In the second and third cases, we wrote the Kirchhoff M/I process as an integration over image point angles. In each of these cases, we recast the integrals over angles as integrals over the source/receiver coordinates. This procedure produced imaging/inversion formulae written as integrations over all sources and receivers. (Although we have only considered horizontal acquisition surfaces here, the extension to curved acquisition surfaces is straightforward, as noted in item 3 in the discussion at the end of section 2.) We have also described how the processing can be organized to lead to output in common opening angle, common azimuth angle at the image point.

For data gathered over parallel lines of multi-streamer cables, Kirchhoff inversion is particularly elusive. However, the Kirchhoff inversions presented in the previous two sections can be applied to these data. We are not aware of any other Kirchhoff inversion for this type of survey.

The full waveform Kirchhoff inversion of the previous section is also of recent derivation. The elements of the integrand in the full waveform inversion formula (33) are appropriate Green's function propagators, the differentiated observed data in the frequency domain and dip-correction factors at the upper surface.

In all cases, we started with deconvolution-type inversion formulae that are shown to be true amplitude in the sense that their peak amplitude on a reflector is in known proportion to the plane-wave reflection coefficient at a determinable incidence angle. Since the transformations employed to obtain correlation-type inversion formulae were exact, those results are the true amplitude in the same sense.

In all cases, the output is separated into COA/CAA panels, ready for amplitude-versus-angle analysis.

Acknowledgments

Guanquan Zhang's research was partially supported by the National Science Foundation of China (10431030). All authors further acknowledge the support and approval for publication of Veritas DGC Inc. Finally, we express our gratitude to John Stockwell of the Center for Wave Phenomena, Colorado School of Mines for a critical reading of this paper.

Appendix A

The purpose of this appendix is to derive equation (7), relating $\mathrm{d}\theta'$ to $\mathrm{d}x_s$. In this discussion, we can dispense with the prime on θ. To begin, we observe that

$$\mathrm{d}\theta = \left|\frac{\mathrm{d}\theta}{\mathrm{d}\alpha_s}\right| \mathrm{d}\alpha_s = \left|\frac{\mathrm{d}\theta}{\mathrm{d}\alpha_s}\right| \left|\frac{\mathrm{d}\alpha_s}{\mathrm{d}x_s}\right| \mathrm{d}x_s. \tag{A.1}$$

As noted in the text, and as can be seen in figure 1,

$$\left|\frac{\mathrm{d}\theta}{\mathrm{d}\alpha}\right| = 1. \tag{A.2}$$

The expression for the 2D Green's function WKBJ amplitude can be found in Bleistein *et al* (2001), as equation (E.4.9),

$$|A(\boldsymbol{y}, \boldsymbol{x})| = \frac{1}{2\sqrt{2\pi J_{2\mathrm{D}}}}, \tag{A.3}$$

with

$$J_{2\mathrm{D}} = \left|\frac{\partial(\boldsymbol{y})}{\partial(\sigma, \theta)}\right| = \frac{1}{v(\boldsymbol{y})}\left|\frac{\partial \boldsymbol{y}}{\partial \theta}\right|. \tag{A.4}$$

In these two equations, $\boldsymbol{y}$ is the Cartesian coordinate along the ray and σ is a standard running parameter along the ray for which

$$\frac{\mathrm{d}\boldsymbol{y}}{\mathrm{d}\sigma} = \boldsymbol{p} = \nabla\tau,$$

with τ the travel time along the ray.

From figure 2, we can see that

$$\left|\frac{\partial \boldsymbol{y}}{\partial \theta}\right| = \left|\frac{\partial x_s}{\partial \theta}\right| \cos\beta_s. \tag{A.5}$$

Now, we use this last result in the expression for $J_{2\mathrm{D}}$ in equation (A.4) to obtain one expression for this function and then solve for $J_{2\mathrm{D}}$ in the amplitude expression (A.3) to obtain the following relationship between the WKBJ amplitude and the derivative of x_s with respect to θ:

$$J_{2\mathrm{D}}\Big|_{y=x_s} = \frac{1}{v(\boldsymbol{x}_s)}\left|\frac{\partial x_s}{\partial \theta}\right| \cos\beta_s = \frac{1}{8\pi A(\boldsymbol{x}_s, \boldsymbol{x})A^*(\boldsymbol{x}_s, \boldsymbol{x})}. \tag{A.6}$$

The scalar x_s in these equations is the x-coordinate of the source position $\boldsymbol{x}_s$. We solve this equation for the derivative of θ with respect to x_s:

$$\left|\frac{\partial \theta}{\partial x_s}\right| = 8\pi A(\boldsymbol{x}_s, \boldsymbol{x})A^*(\boldsymbol{x}_s, \boldsymbol{x})\frac{\cos\beta_s}{v(\boldsymbol{x}_s)}. \tag{A.7}$$

This is equivalent to the equality in equation (7) for $\mathrm{d}\theta$.

Appendix B

In this appendix, we derive equation (13) relating the differential area on the unit sphere of migration angles and the differential surface area element in source points on the acquisition surface.

We use a 3D right-handed coordinate system with the z-axis facing downwards as in figure 3. The notation will be as follows:

Source point: denoted by $\boldsymbol{x}_s = (x_{1s}, x_{2s}, 0)$.
Image point: denoted by $\boldsymbol{x} = (x_1, x_2, x_3)$.
Migration dip direction: defined by a unit vector $\hat{\boldsymbol{\nu}}$ at the image point.

$$\hat{\boldsymbol{\nu}} = (\cos\nu_2 \sin\nu_1, \sin\nu_2 \sin\nu_1, \cos\nu_1). \tag{B.1}$$

Below, we follow this same convention with angles: the polar angle will have subscript 1 and the azimuthal angle will have subscript 2.

The running Cartesian coordinate along the ray: ... from $\boldsymbol{x}$ to $\boldsymbol{x}_s$. Denoted by $\boldsymbol{y}$.
Ray direction at the image point:

$$\hat{\boldsymbol{\alpha}}_s = (\cos\alpha_{s2}\sin\alpha_{s1}, \sin\alpha_{s2}\sin\alpha_{s1}, \cos\alpha_{s1}). \tag{B.2}$$

Ray direction at the source:

$$\hat{\boldsymbol{\beta}}_s = (\cos\beta_{s2}\sin\beta_{s1}, \sin\beta_{s2}\sin\beta_{s1}, \cos\beta_{s1}). \tag{B.3}$$

θ is the angle between the vector $\hat{\boldsymbol{\alpha}}_s$ and the vector $\hat{\boldsymbol{\nu}}$. Further, $\hat{\boldsymbol{\alpha}}_s$ depends on ϕ, the rotation around $\hat{\boldsymbol{\nu}}$. The initial orientation ($\phi = 0$) is undefined. We show below that the result is independent of this initial orientation.

We need to carry out an integration over θ and ϕ for fixed $\hat{\boldsymbol{\nu}}$. In this case, $\boldsymbol{x}_s$ varies and we seek the Jacobian associated with the change of variables from θ and ϕ to the two nonzero coordinates of $\boldsymbol{x}_s$—x_{s1} and x_{s2}.

It is necessary to compute the 2×2 Jacobian in the identity

$$\mathrm{d}\theta\mathrm{d}\phi = \left|\frac{\partial(\theta,\phi)}{\partial(x_{s1},x_{s2})}\right| \mathrm{d}x_{s1}\,\mathrm{d}x_{s2}. \tag{B.4}$$

We first use the chain rule for Jacobians to set

$$\frac{\partial(x_1,x_2)}{\partial(\theta,\phi)} = \frac{\partial(x_1,x_2)}{\partial(\alpha_{s1},\alpha_{s2})}\frac{\partial(\alpha_{s1},\alpha_{s2})}{\partial(\theta,\phi)}. \tag{B.5}$$

The first Jacobian on the right-hand side is a cofactor of the 3D Jacobian of ray theory and therefore can be written in terms of the ray amplitude. The second Jacobian provides the scale between a differential element in (θ,ϕ) and a differential element in the angles $(\alpha_{s1},\alpha_{s2})$. Below, we derive those relationships in detail.

B.1. Analysis of the first factor $\partial(x_1,x_2)/\partial(\alpha_{s1},\alpha_{s2})$, the space–angle transformation Jacobian, in equation (B.5)

Here we derive an expression for the first Jacobian on the right-hand side in equation (B.5) in terms of the Green's function ray amplitude. The starting point for this derivation is equation (E.4.2) in Bleistein *et al* (2001). In the notation of this paper, that result is

$$|A(\boldsymbol{y},\boldsymbol{x})| = \frac{1}{4\pi}\sqrt{\frac{\sin\alpha_{s1}}{v(\boldsymbol{x})J_{3\mathrm{D}}}}. \tag{B.6}$$

In this equation, v is the wave speed and

$$J_{3\mathrm{D}} = \left|\frac{\mathrm{d}\boldsymbol{y}}{\mathrm{d}\sigma}\cdot\frac{\mathrm{d}\boldsymbol{y}}{\mathrm{d}\alpha_{s1}}\times\frac{\mathrm{d}\boldsymbol{y}}{\mathrm{d}\alpha_{s2}}\right|. \tag{B.7}$$

The variable σ is a running parameter along the ray for which

$$\frac{\mathrm{d}\boldsymbol{y}}{\mathrm{d}\sigma} = \boldsymbol{p} = \nabla\tau,$$

with τ the travel time along the ray.

The cross product in equation (B.7) is in the direction of the σ derivative, so that

$$J_{3\mathrm{D}} = |\nabla\tau|\left|\frac{\mathrm{d}\boldsymbol{y}}{\mathrm{d}\alpha_{s1}}\times\frac{\mathrm{d}\boldsymbol{y}}{\mathrm{d}\alpha_{s2}}\right| = \frac{1}{v(\boldsymbol{y})}\left|\frac{\mathrm{d}\boldsymbol{y}}{\mathrm{d}\alpha_{s1}}\times\frac{\mathrm{d}\boldsymbol{y}}{\mathrm{d}\alpha_{s2}}\right|. \tag{B.8}$$

The product

$$\left|\frac{\mathrm{d}\boldsymbol{y}}{\mathrm{d}\alpha_{s1}}\times\frac{\mathrm{d}\boldsymbol{y}}{\mathrm{d}\alpha_{s2}}\right| \mathrm{d}\alpha_{s1}\,\mathrm{d}\alpha_{s2}$$

is the area of the differential cross section at the point $\boldsymbol{y}$. When $\boldsymbol{y} = \boldsymbol{x}_s$, this area can be expressed in terms of the differential area cut out on the acquisition surface. As in figure 2 showing the differential areas of interest in 2D, it is also true in 3D that

$$\left|\frac{\mathrm{d}\boldsymbol{y}}{\mathrm{d}\alpha_{s1}} \times \frac{\mathrm{d}\boldsymbol{y}}{\mathrm{d}\alpha_{s2}}\right|\Big|_{\boldsymbol{y}=\boldsymbol{x}_s} = \left|\frac{\partial(x_{s1}, x_{s2})}{\partial(\alpha_1, \alpha_2)}\right| \cos\beta_{s1}. \tag{B.9}$$

Here, we have dropped the product $\mathrm{d}\alpha_{s1}\,\mathrm{d}\alpha_{s2}$ that appears on both sides of the equation when equating areas. Thus, combining the results of equation (B.5)–(B.8), we find that

$$J_{3\mathrm{D}} = \frac{\cos\beta_{s1}}{v(\boldsymbol{x}_s)}\left|\frac{\partial(x_{s1}, x_{s2})}{\partial(\alpha_1, \alpha_2)}\right| = \frac{\sin\alpha_{s1}}{16\pi^2 A(\boldsymbol{x}_s, \boldsymbol{x})A^*(\boldsymbol{x}_s, \boldsymbol{x})v(\boldsymbol{x})}. \tag{B.10}$$

Now solve for the 2×2 Jacobian here:

$$\left|\frac{\partial(\alpha_{s1}, \alpha_{s2})}{\partial(x_{s1}, x_{s2})}\right| = \frac{\cos\beta_{s1}}{v(\boldsymbol{x}_s)}\frac{16\pi^2 A(\boldsymbol{x}_s, \boldsymbol{x})A^*(\boldsymbol{x}_s, \boldsymbol{x})v(\boldsymbol{x})}{\sin\alpha_{s1}}. \tag{B.11}$$

This is the result we need for the first Jacobian on the right-hand side of equation (B.5).

B.2. Analysis of the first factor $\partial(\alpha_{s1}, \alpha_{s2})/\partial(\theta, \phi)$, the angle–angle transformation Jacobian, in equation (B.5)

We turn now to the analysis of the second Jacobian in equation (B.5). We note that the representation of the vector $\hat{\boldsymbol{\alpha}}_s$ in a coordinate system with $\hat{\boldsymbol{\nu}}$ as the third axis of a right-handed coordinate system is fairly straightforward. Thus, we will begin by examining the transformations that get us there.

In the original Cartesian coordinate system of figure 3, let us introduce the three basis vectors, $\boldsymbol{x}_1, \boldsymbol{x}_2, \boldsymbol{x}_3$. We will transform this basis into one for which the third basis vector is $\hat{\boldsymbol{\nu}}$. We do this in two steps. First, introduce a new coordinate system with basis vectors $\boldsymbol{x}_1', \boldsymbol{x}_2', \boldsymbol{x}_3'$, obtained from the original coordinate system by a rotation through the angle ν_2 about the vector $\boldsymbol{x}_3$. This is an orthogonal transformation that can be represented by

$$\begin{bmatrix}\boldsymbol{x}_1'\\ \boldsymbol{x}_2'\\ \boldsymbol{x}_3'\end{bmatrix} = T_2\begin{bmatrix}\boldsymbol{x}_1\\ \boldsymbol{x}_2\\ \boldsymbol{x}_3\end{bmatrix}, \qquad T_2 = \begin{bmatrix}\cos\nu_2 & \sin\nu_2 & 0\\ -\sin\nu_2 & \cos\nu_2 & 0\\ 0 & 0 & 1\end{bmatrix}. \tag{B.12}$$

Next, introduce a new coordinate system with basis vectors $\boldsymbol{x}_1'', \boldsymbol{x}_2'', \boldsymbol{x}_3''$, obtained from the previous one by rotation about the vector $\boldsymbol{x}_2'$ through an angle ν_1. This is also an orthogonal transformation. It can be represented by

$$\begin{bmatrix}\boldsymbol{x}_1''\\ \boldsymbol{x}_2''\\ \boldsymbol{x}_3''\end{bmatrix} = T_1\begin{bmatrix}\boldsymbol{x}_1'\\ \boldsymbol{x}_2'\\ \boldsymbol{x}_3'\end{bmatrix}, \qquad T_1 = \begin{bmatrix}\cos\nu_1 & 0 & -\sin\nu_1\\ 0 & 1 & 0\\ \sin\nu_1 & 0 & \cos\nu_1\end{bmatrix}. \tag{B.13}$$

In terms of this new coordinate system, we can write

$$\hat{\boldsymbol{\alpha}}_s = \begin{bmatrix}\sin\theta\cos(\phi-\phi_0)\\ \sin\theta\sin(\phi-\phi_0)\\ \cos\theta\end{bmatrix}^T\begin{bmatrix}\boldsymbol{x}_1''\\ \boldsymbol{x}_2''\\ \boldsymbol{x}_3''\end{bmatrix}. \tag{B.14}$$

In this equation and below, the superscript T denotes transpose. Further, ϕ_0 denotes a constant shift in ϕ because we do not know the orientation of the $\{''\}$ axes with respect to the zero value of ϕ. It will not matter in the end because we will see that the Jacobian we seek is independent of $\phi - \phi_0$.

Now we need to use the transformations in equations (B.12) and (B.13) to back substitute and write a result for $\hat{\boldsymbol{\alpha}}_s$ in terms of the original coordinates where we know the representation of $\hat{\boldsymbol{\alpha}}_s$:

$$\hat{\boldsymbol{\alpha}}_s = \begin{bmatrix} \sin\theta\cos(\phi-\phi_0) \\ \sin\theta\sin(\phi-\phi_0) \\ \cos\theta \end{bmatrix}^T T_1 T_2 \begin{bmatrix} \boldsymbol{x}_1 \\ \boldsymbol{x}_2 \\ \boldsymbol{x}_3 \end{bmatrix} = \begin{bmatrix} \sin\alpha_{s1}\cos\alpha_{s2} \\ \sin\alpha_{s1}\sin\alpha_{s2} \\ \cos\alpha_{s1} \end{bmatrix}^T \begin{bmatrix} \boldsymbol{x}_1 \\ \boldsymbol{x}_2 \\ \boldsymbol{x}_3 \end{bmatrix}. \tag{B.15}$$

We invert this equation to solve for $\hat{\boldsymbol{\alpha}}_s$:

$$T_2^T T_1^T \begin{bmatrix} \sin\theta\cos(\phi-\phi_0) \\ \sin\theta\sin(\phi-\phi_0) \\ \cos\theta \end{bmatrix} = \begin{bmatrix} \sin\alpha_{s1}\cos\alpha_{s2} \\ \sin\alpha_{s1}\sin\alpha_{s2} \\ \cos\alpha_{s1} \end{bmatrix}. \tag{B.16}$$

Next, we need to take the derivatives of this last equation with respect to θ and ϕ. Differentiation with respect to θ leads to the equation

$$T_2^T T_1^T \begin{bmatrix} \cos\theta\cos(\phi-\phi_0) \\ \cos\theta\sin(\phi-\phi_0) \\ -\sin\theta \end{bmatrix} = \frac{\partial\alpha_{s1}}{\partial\theta} \begin{bmatrix} \cos\alpha_{s1}\cos\alpha_{s2} \\ \cos\alpha_{s1}\sin\alpha_{s2} \\ -\sin\alpha_{s1} \end{bmatrix} + \frac{\partial\alpha_{s2}}{\partial\theta} \begin{bmatrix} -\sin\alpha_{s1}\sin\alpha_{s2} \\ \sin\alpha_{s1}\cos\alpha_{s2} \\ 0 \end{bmatrix}. \tag{B.17}$$

With an appropriate matrix multiplication—effectively a dot product—we can solve for the two derivatives here as follows:

$$\begin{bmatrix} \cos\alpha_{s1}\cos\alpha_{s2} \\ \cos\alpha_{s1}\sin\alpha_{s2} \\ -\sin\alpha_{s1} \end{bmatrix}^T T_2^T T_1^T \begin{bmatrix} \cos\theta\cos(\phi-\phi_0) \\ \cos\theta\sin(\phi-\phi_0) \\ -\sin\theta \end{bmatrix} = \frac{\partial\alpha_{s1}}{\partial\theta}, \tag{B.18}$$

and

$$\begin{bmatrix} -\sin\alpha_{s2} \\ \cos\alpha_{s2} \\ 0 \end{bmatrix}^T T_2^T T_1^T \begin{bmatrix} \cos\theta\cos(\phi-\phi_0) \\ \cos\theta\sin(\phi-\phi_0) \\ -\sin\theta \end{bmatrix} = \sin\alpha_{s1}\frac{\partial\alpha_{s2}}{\partial\theta}. \tag{B.19}$$

Now, we repeat the process with the ϕ derivative of the vector equality of equation (B.16). As a first step,

$$T_2^T T_1^T \begin{bmatrix} -\sin\theta\sin(\phi-\phi_0) \\ \sin\theta\cos(\phi-\phi_0) \\ 0 \end{bmatrix} = \frac{\partial\alpha_{s1}}{\partial\phi} \begin{bmatrix} \cos\alpha_{s1}\cos\alpha_{s2} \\ \cos\alpha_{s1}\sin\alpha_{s2} \\ -\sin\alpha_{s1} \end{bmatrix} + \frac{\partial\alpha_{s2}}{\partial\phi} \begin{bmatrix} -\sin\alpha_{s1}\sin\alpha_{s2} \\ \sin\alpha_{s1}\cos\alpha_{s2} \\ 0 \end{bmatrix}. \tag{B.20}$$

Next, we repeat the matrix multiplication used above,

$$\begin{bmatrix} \cos\alpha_{s1}\cos\alpha_{s2} \\ \cos\alpha_{s1}\sin\alpha_{s2} \\ -\sin\alpha_{s1} \end{bmatrix}^T T_2^T T_1^T \begin{bmatrix} -\sin\theta\sin(\phi-\phi_0) \\ \sin\theta\cos(\phi-\phi_0) \\ 0 \end{bmatrix} = \frac{\partial\alpha_{s1}}{\partial\phi}, \tag{B.21}$$

and

$$\begin{bmatrix} -\sin\alpha_{s2} \\ \cos\alpha_{s2} \\ 0 \end{bmatrix}^T T_2^T T_1^T \begin{bmatrix} -\sin\theta\sin(\phi-\phi_0) \\ \sin\theta\cos(\phi-\phi_0) \\ 0 \end{bmatrix} = \sin\alpha_{s1}\frac{\partial\alpha_{s2}}{\partial\phi}. \tag{B.22}$$

Note that the two multipliers that we used are the unit vectors along the angular directions of the unit sphere centred at $\boldsymbol{x}$, containing $\hat{\boldsymbol{\alpha}}_s$. On the other hand, the right-hand side of equation (B.16) is the normal vector outward from the same sphere, so that these three vectors are orthogonal. This allows us to express the Jacobian we seek as the determinant of a 3×3

matrix, as follows:

$$\begin{bmatrix} \cos\alpha_{s1}\cos\alpha_{s2} & \cos\alpha_{s1}\sin\alpha_{s2} & -\sin\alpha_{s1} \\ -\sin\alpha_{s2} & \cos\alpha_{s2} & 0 \\ \sin\alpha_{s1}\cos\alpha_{s2} & \sin\alpha_{s1}\sin\alpha_{s2} & \cos\alpha_{s2} \end{bmatrix} T_2^T T_1^T$$
$$\cdot \begin{bmatrix} \cos\theta\cos(\phi-\phi_0) & -\sin\theta\sin(\phi-\phi_0) & \sin\theta\cos(\phi-\phi_0) \\ \cos\theta\sin(\phi-\phi_0) & \sin\theta\cos(\phi-\phi_0) & \sin\theta\sin(\phi-\phi_0) \\ -\sin\theta & 0 & \cos\theta \end{bmatrix}$$
$$= \begin{bmatrix} \partial\alpha_{s1}/\partial\theta & \partial\alpha_{s1}/\partial\phi & 0 \\ \sin\alpha_{s1}(\partial\alpha_{s2}/\partial\theta) & \sin\alpha_{s1}(\partial\alpha_{s2}/\partial\phi) & 0 \\ 0 & 0 & 1 \end{bmatrix}. \quad \text{(B.23)}$$

The first three matrices on the left-hand side all have determinant equal to 1, while the last matrix has determinant equal to $\sin\theta$ (independent of $\phi-\phi_0$ as promised!). Consequently,

$$\left|\frac{\partial(\alpha_{s1},\alpha_{s2})}{\partial(\theta,\phi)}\right| = \frac{\sin\theta}{\sin\alpha_{s1}}. \quad \text{(B.24)}$$

We use this result with equation (B.11), the expression for the Jacobian relating the angles α_{s1} and α_{s2} to the source coordinates, in the Jacobian relating those source coordinates to the dip and azimuthal angles equation (B.5). This, in turn, is substituted into the expression for $\mathrm{d}\theta\,\mathrm{d}\phi$, equation (B.4), to obtain equation (13), the expression for the differential area element $\sin\theta'\,\mathrm{d}\theta'\,\mathrm{d}\phi'$ in terms of the differential element in source point coordinates.

Appendix C. Change of variables from four image point angles to source and receiver coordinates

In section 3, equation (19) is a reflectivity formula as an integral in four angular variables at the image point. Following that, we rewrote the reflectivity function in equation (20) as an integral in source/receiver coordinates. In this appendix, we derive the Jacobian of transformation that allows us to effect that change of variables, that is, to rewrite the integral in variables $\nu_1, \nu_2, \theta, \phi$ as an integral in the variables $x_{s1}, x_{s2}, x_{r1}, x_{r2}$. As a first step, we use the chain rule for Jacobians to write

$$\frac{\partial(\nu_1,\nu_2,\theta,\phi)}{\partial(x_{s1},x_{s2},x_{r1},x_{r2})} = \frac{\partial(\alpha_{s1},\alpha_{s2},\alpha_{r1},\alpha_{r2})}{\partial(x_{s1},x_{s2},x_{r1},x_{r2})}\frac{\partial(\nu_1,\nu_2,\theta,\phi)}{\partial(\alpha_{s1},\alpha_{s2},\alpha_{r1},\alpha_{r2})}. \quad \text{(C.1)}$$

Let us consider the first factor on the right-hand side here and observe that the direction of the ray from the source to the image point depends on the location of the source and not on the location of the receiver. Therefore, α_{s1} and α_{s2} are functions of x_{s1} and x_{s2} and not functions of x_{r1} and x_{r2}. Similarly, α_{r1} and α_{r2} are functions of x_{r1} and x_{r2} and not functions of x_{s1} and x_{s2}. Thus, the first Jacobian has the anti-diagonally 2×2 corners consisting only of zeros and the 4×4 Jacobian is really a product of two 2×2 Jacobians, namely

$$\frac{\partial(\alpha_{s1},\alpha_{s2},\alpha_{r1},\alpha_{r2})}{\partial(x_{s1},x_{s2},x_{r1},x_{r2})} = \frac{\partial(\alpha_{s1},\alpha_{s2})}{\partial(x_{s1},x_{s2})}\frac{\partial(\alpha_{r1},\alpha_{r2})}{\partial(x_{r1},x_{r2})}. \quad \text{(C.2)}$$

The first Jacobian on the right-hand side here has been rewritten in terms of Green's function amplitudes in appendix B, namely, as equation (B.11). Of course, by replacing s by r in that formula, we obtain the right result for the second factor. Thus,

$$\frac{\partial(\alpha_{s1},\alpha_{s2},\alpha_{r1},\alpha_{r2})}{\partial(x_{s1},x_{s2},x_{r1},x_{r2})} = [16\pi^2]^2\frac{\cos\beta_{s1}}{\sin\alpha_{s1}}\frac{\cos\beta_{r1}}{\sin\alpha_{r1}}\frac{v(\boldsymbol{x})}{v(\boldsymbol{x}_s)}\frac{v(\boldsymbol{x})}{v(\boldsymbol{x}_r)}$$
$$\cdot A(\boldsymbol{x}_s,\boldsymbol{x})A^*(\boldsymbol{x}_s,\boldsymbol{x})A(\boldsymbol{x}_r,\boldsymbol{x})A^*(\boldsymbol{x}_r,\boldsymbol{x}). \quad \text{(C.3)}$$

The second Jacobian on the right-hand side in equation (C.1) is more complicated. A formula can be found in Burridge *et al* (1998). However, we prefer a simpler representation. Note that this expression is independent of the background model; it only depends on the transformations between various coordinate systems at the image point.

We actually calculate the inverse of the Jacobian we need for equation (C.1). The individual elements of that Jacobian can all be calculated following the method of appendix B. The result is surprisingly simple, namely,

$$\frac{\partial(\alpha_{s1}, \alpha_{s2}, \alpha_{r1}, \alpha_{r2})}{\partial(\nu_1, \nu_2, \theta, \phi)} = 2\frac{\sin 2\theta \sin \nu_1}{\sin \alpha_{s1} \sin \alpha_{s2}}. \tag{C.4}$$

We combine this result with equation (C.3), the Jacobian relating initial ray direction angles to image point angles in the expression for the Jacobian relating image point angles and source and receiver coordinates (C.1) to conclude that

$$\begin{aligned}\sin \nu_1 \, \mathrm{d}\nu_1 \, \mathrm{d}\nu_2 \, \mathrm{d}\theta \, \mathrm{d}\phi &= \frac{\partial(\nu_1, \nu_2, \theta, \phi)}{\partial(x_{s1}, x_{s2}, x_{r1}, x_{r2})} \, \mathrm{d}x_{s1} \, \mathrm{d}x_{s2} \, \mathrm{d}x_{r1} \, \mathrm{d}x_{r2} \\ &= [16\pi^2]^2 \frac{\cos \beta_{s1}}{v(\boldsymbol{x}_s)} \frac{\cos \beta_{r1}}{v(\boldsymbol{x}_r)} \frac{v^2(\boldsymbol{x})}{2 \sin 2\theta} \\ &\quad \cdot A(\boldsymbol{x}_s, \boldsymbol{x}) A^*(\boldsymbol{x}_s, \boldsymbol{x}) A(\boldsymbol{x}_r, \boldsymbol{x}) A^*(\boldsymbol{x}_r, \boldsymbol{x}) \, \mathrm{d}x_{s1} \, \mathrm{d}x_{s2} \, \mathrm{d}x_{r1} \, \mathrm{d}x_{r2}. \end{aligned} \tag{C.5}$$

When this result is used in equation (19), the reflectivity as an integral in angular variables, we obtain equation (20) as an expression of the reflectivity as an integral in source/receiver coordinates.

Appendix D. The Kirchhoff-approximate upward-propagating wave with full waveform Green's functions

In this appendix, we outline the development of the integral formula for the Kirchhoff-approximate upward scattered field response from a single reflector.

Forward modelling via the Kirchhoff approximation starts from two assumptions relating the incident and reflected field at a point on the reflecting surface. These two approximations can be written in the form

$$u_R = RF(\omega)G_s, \qquad \frac{\partial u_R}{\partial n} = -RF(\omega)\frac{\partial G_s}{\partial n}, \quad \text{on } S. \tag{D.1}$$

In this equation, u_R is the reflected wavefield and $F(\omega)G_s$ is the incident wavefield from the source. Since we assume a point source, G_s is just Green's function from the source point $\boldsymbol{x}_s$ to the reflecting surface S, while $F(\omega)$ is the source signature. The derivatives here are upward normal derivatives at the reflector.

When we use ray theory,

$$G_s \sim A_s \exp(\mathrm{i}\omega\tau_s + \mathrm{i}\pi/2 \cdot \mathsf{K_s}(\boldsymbol{x}', \boldsymbol{x}_s)), \tag{D.2}$$

with τ_s and A_s the WKBJ travel time and amplitude; $\mathsf{K_s}$ is the KMAH index for the ray trajectory from $\boldsymbol{x}_s$ to $\boldsymbol{x}'$. This index is a count of the number of caustics that the ray trajectory encounters on its travel path from the source to image point. The phase adjustment $\mathrm{i}\pi/2$ accounts for the change in waveform signature as the wave passes each caustic. The phase adjustment $\mathrm{i}\pi/2\mathsf{K_s}(\boldsymbol{x}', \boldsymbol{x}_s)$ in equation (D.2) accumulates the total phase shift on the trajectory. Furthermore, $\boldsymbol{x}'$ is the Cartesian coordinate of the point on the reflecting surface. In this case, we use the further approximation in equation (D.1),

$$\frac{\partial G_s}{\partial n} \sim \mathrm{i}\omega\hat{\boldsymbol{n}} \cdot \nabla\tau_s G_s. \tag{D.3}$$

We will employ this approximation, even when using other than ray-theoretic Green's functions.

These approximations are used in an exact forward modelling formula for the reflected field at any point above the reflector written in terms of its values on the reflector:

$$u_R(\boldsymbol{x}_r, \boldsymbol{x}_s, \omega) = F(\omega)\int_S \left\{u_R(\boldsymbol{x}', \boldsymbol{x}_s, \omega)\frac{\partial G_r(\boldsymbol{x}_r, \boldsymbol{x}', \omega)}{\partial n} - G_r(\boldsymbol{x}_r, \boldsymbol{x}', \omega)\frac{\partial u_R(\boldsymbol{x}', \boldsymbol{x}_s, \omega)}{\partial n}\right\}\mathrm{d}S$$

$$\sim F(\omega)\int_S R\left\{G_s(\boldsymbol{x}', \boldsymbol{x}_s, \omega)\frac{\partial G_r(\boldsymbol{x}_r, \boldsymbol{x}', \omega)}{\partial n} + G_r(\boldsymbol{x}_r, \boldsymbol{x}', \omega)\frac{\partial G_s(\boldsymbol{x}', \boldsymbol{x}_s, \omega)}{\partial n}\right\}\mathrm{d}S. \quad \text{(D.4)}$$

Here, $\boldsymbol{x}_r$ is the 'receiver point' at which the field is observed; $G_r(\boldsymbol{x}_r, \boldsymbol{x}', \omega)$ is Green's function that evaluates the field at $\boldsymbol{x}_r$. It is important that the arguments be in the indicated order here. This function starts out as $G_r^\dagger(\boldsymbol{x}', \boldsymbol{x}_r, \omega)$ with † denoting 'adjoint'. While the acoustic wave equation with constant density is self-adjoint, which is not true in general. Thus, the Green's theorem representation of the wavefield must acknowledge the general derivation and use Green's function of the adjoint equation. It is then a standard identity that allows us to replace the adjoint Green's function with Green's function of the direct equation but interchanged arguments.

The next step is to replace the surface integral in the last equation above by a volume integral. Before we can do that, it is necessary to remove the normal derivative in that equation. To do so, we first use the WKBJ approximation (D.3) to rewrite the upward propagating wave representation (D.4) as

$$u_R(\boldsymbol{x}_r, \boldsymbol{x}_s, \omega) \sim \mathrm{i}\omega F(\omega)\int_S R\hat{\boldsymbol{n}}\cdot\nabla_y\tau G_s(\boldsymbol{x}', \boldsymbol{x}_s, \omega)G_r(\boldsymbol{x}_r, \boldsymbol{x}', \omega)\,\mathrm{d}S, \quad \tau = \tau_s + \tau_r. \quad \text{(D.5)}$$

Now, we further simplify this result by observing that at the stationary point(s) of the integration, $\hat{\boldsymbol{n}}$ and $\nabla_y\tau$ are colinear but point in opposite directions:

$$\hat{\boldsymbol{n}}\cdot\nabla_{x'}\tau = -|\nabla_{x'}\tau|. \quad \text{(D.6)}$$

Therefore, we can rewrite equation (D.5) as

$$u_R(\boldsymbol{x}_r, \boldsymbol{x}_s, \omega) \sim -\mathrm{i}\omega F(\omega)\int_S R|\nabla_{x'}\tau|G_s(\boldsymbol{x}', \boldsymbol{x}_s, \omega)G_r(\boldsymbol{x}_r, \boldsymbol{x}', \omega)\,\mathrm{d}S. \quad \text{(D.7)}$$

Next, we introduce the *singular function* of the reflection surface denoted by $\gamma(\boldsymbol{x}')$ in Bleistein *et al* (2001). This is a delta-function of normal distance to the surface. Further, the product $R\gamma$ is what we mean by the *reflectivity* function denoted by $\mathcal{R}(\boldsymbol{x}')$. What matters to us here is that $\mathrm{d}n\,\mathrm{d}S = \mathrm{d}V$ and $\int\{\cdot\}\gamma\,\mathrm{d}V = \int\{\cdot\}\,\mathrm{d}S$; that is, the introduction of $\gamma\,\mathrm{d}n$ and another integration transforms the surface integral into a volume integral in the variables, $\boldsymbol{x}'$.

The second representation of the upward propagating wave equation (D.4) is now recast as equation (22).

Appendix E. Asymptotic analysis of the norm $\|(K^\dagger K)^{-1}\|$

We describe the asymptotic analysis of the operator norm equation (26) in this appendix. First, we replace Green's functions by their ray-theoretic equivalents. Then, equation (26) becomes

$$\|(K^\dagger K)^{-1}\| = \left|\int \mathrm{d}^2\xi\,\mathrm{d}\omega\int \mathrm{d}V\omega^2|\nabla_{x'}\tau(\boldsymbol{x}', \boldsymbol{\xi})|A_s^*(\boldsymbol{x}_s, \boldsymbol{x})A_r^*(\boldsymbol{x}, \boldsymbol{x}_r)\right.$$

$$\left.\cdot\,|\nabla_x\tau(\boldsymbol{x}, \boldsymbol{\xi})|A_s(\boldsymbol{x}', \boldsymbol{x}_s)A_r(\boldsymbol{x}_r, \boldsymbol{x}')\exp(\mathrm{i}\omega\{\tau(\boldsymbol{x}', \boldsymbol{\xi}) - \tau(\boldsymbol{x}, \boldsymbol{\xi})\})\right|^{-1}, \quad \text{(E.1)}$$

independent of the KMAH index.

Observe in this last equation that when $\boldsymbol{x}' = \boldsymbol{x}$ the phase is zero and the integration over $\boldsymbol{\xi}$ has no oscillation at all. This point is a critical point of the integrand. In fact, it is the

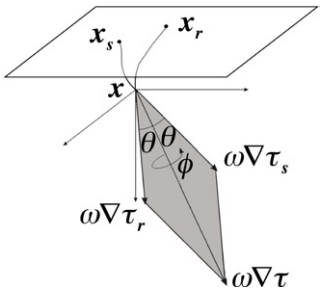

Figure 4. Coordinates of the 2D inversion process. $\boldsymbol{x}$: the image point. $\boldsymbol{x}_s$ and $\boldsymbol{x}_r$: the source and specular receiver, respectively. θ: incident specular angle of the source ray, also the reflection angle with respect to the normal. $\nabla\tau_s$ and $\nabla\tau_r$: gradients of travel time from the source and receiver, respectively, with sum $\nabla\tau$. As previously in the text, θ and ϕ are the half-opening angle between the rays and azimuth angle of the plane of the rays, as indicated.

dominant critical point and leads to the leading-order approximation of this integral. Thus, we can approximate the amplitude here by setting $\boldsymbol{x}' = \boldsymbol{x}$ and we approximate the travel time difference in the phase by the linear term in its Taylor series, namely,

$$\omega\{\tau(\boldsymbol{x}', \boldsymbol{\xi}) - \tau(\boldsymbol{x}, \boldsymbol{\xi})\} \approx \boldsymbol{k} \cdot (\boldsymbol{x}' - \boldsymbol{x}), \qquad \boldsymbol{k} = \omega\nabla_x\tau(\boldsymbol{x}, \boldsymbol{\xi}). \tag{E.2}$$

We take this last expression as the definition of a change of variables of integration from $\boldsymbol{\xi}, \omega$ to $\boldsymbol{k}$ and remark that this can be made exact in a neighbourhood of the critical point. This identity is fundamental to the Kirchhoff M/I theory; see figure 4 where the wave vector $\omega\nabla\tau$ is depicted. For a fixed image point, as the source/receiver pairs vary, both the magnitude and direction of $\boldsymbol{k}$ vary along some surface. When ω ranges over its bandwidth, a volume in the $\boldsymbol{k}$ domain is generated; this is the limited aperture over which data are available in this spatial Fourier domain generated by the source/receiver configuration and the bandwidth. For different imaging points, the $\boldsymbol{k}$ domain aperture changes because the suite of gradients of travel times changes. In this sense, the aperture of information available for inversion is a *micro-local* property. The direction of $\boldsymbol{k}$ is called the migration dip. The direction of the reflector normal is called the reflection dip. It is a fundamental consequence of the theory that one can only image a reflector at a point $\boldsymbol{x}$ if the reflector dip lies in the aperture of migration dips provided by the acquisition geometry.

In terms of the new variables of integration and approximations, the norm representation (E.1) becomes

$$\|(K^\dagger K)^{-1}\| = \left| \int \mathrm{d}^3k \int \mathrm{d}V \, |\nabla_x\tau(\boldsymbol{x}, \boldsymbol{\xi})| A_s(\boldsymbol{x}, \boldsymbol{x}_s) A_r(\boldsymbol{x}_r, \boldsymbol{x})|^2 \omega^2 \right.$$
$$\left. \times \left| \frac{\partial(\boldsymbol{\xi}, \omega)}{\partial(\boldsymbol{k})} \right| \exp(\mathrm{i}\boldsymbol{k} \cdot (\boldsymbol{x}' - \boldsymbol{x})) \right|^{-1}. \tag{E.3}$$

It is easier to write down the inverse of the Jacobian of transformation from the variables $\boldsymbol{\xi}, \omega$ to $\boldsymbol{k}$ than to calculate the indicated Jacobian under the integral sign here. For that purpose, we use the definition of $\boldsymbol{k}$ in equation (E.2). The result is

$$\frac{\partial(\boldsymbol{k})}{\partial(\boldsymbol{\xi}, \omega)} = \omega^2 \det \begin{bmatrix} \nabla_x\tau(\boldsymbol{x}, \boldsymbol{\xi}) \\ \dfrac{\partial\nabla_x\tau(\boldsymbol{x}, \boldsymbol{\xi})}{\partial\xi_1} \\ \dfrac{\partial\nabla_x\tau(\boldsymbol{x}, \boldsymbol{\xi})}{\partial\xi_2} \end{bmatrix} = \omega^2 h(\boldsymbol{x}, \boldsymbol{\xi}). \tag{E.4}$$

In this equation $h(\boldsymbol{x}, \boldsymbol{\xi})$ is the usual Beylkin determinant.

Using this result in norm representation (E.3) leads to the result

$$\|(K^\dagger K)^{-1}\| = \left| \int \mathrm{d}^3k \int \mathrm{d}V \, |\nabla_x \tau(\boldsymbol{x}, \boldsymbol{\xi})| A_s(\boldsymbol{x}, \boldsymbol{x}_s) A_r(\boldsymbol{x}_r, \boldsymbol{x})|^2 \, |h(\boldsymbol{x}, \boldsymbol{\xi})|^{-1} \, \mathrm{e}^{\mathrm{i}\boldsymbol{k}\cdot(\boldsymbol{x}'-\boldsymbol{x})} \right|^{-1}. \tag{E.5}$$

In this integral, note that ω appears in the phase in $\boldsymbol{k}$, but no longer appears in the amplitude, which then is a function of $\boldsymbol{\xi}(\boldsymbol{k})$. It is a remarkable fact of the change of variables defined in equation (E.2) that, except for sign(ω), $\boldsymbol{\xi}$ is a function of the direction of $\boldsymbol{k}$ and independent of its magnitude. To see this, simply divide $\boldsymbol{k}$ in equation (E.2) by its magnitude to determine that

$$\hat{\boldsymbol{k}} = \frac{\boldsymbol{k}}{|\boldsymbol{k}|} = \mathrm{sign}(\omega) \frac{\nabla_x \tau(\boldsymbol{x}, \boldsymbol{\xi})}{|\nabla_x \tau(\boldsymbol{x}, \boldsymbol{\xi})|} = \mathrm{sign}(\omega) \hat{\boldsymbol{\nu}}, \tag{E.6}$$

with $\hat{\boldsymbol{\nu}}$ defined in figure 3. Both choices of $\hat{\boldsymbol{k}}$ correspond to the same migration dip, hence, the same $\boldsymbol{\xi}$; so sign(ω) has no effect on the amplitude of the integrand in equation (E.5), our last expression for the norm we seek. Consequently, the only dependence on $k = |\boldsymbol{k}|$ in the integrand is in the phase. This suggests that we would be better off analysing this integral in spherical polar coordinates. We introduce k and two spherical polar angles, ν_1 and ν_2, with ν_1 measured from the line defined by $\boldsymbol{x}' - \boldsymbol{x}$. In this case,

$$\mathrm{d}^3k = k^2 \sin\nu_1 \, \mathrm{d}\nu_1 \, \mathrm{d}\nu_2 \, \mathrm{d}k,$$

and the k-domain integration in the norm representation (E.5) takes the form

$$\int \mathrm{d}^3k \cdots \mathrm{e}^{\mathrm{i}\boldsymbol{k}\cdot(\boldsymbol{x}'-\boldsymbol{x})} = \int k^2 \sin\nu_1 \, \mathrm{d}\nu_1 \, \mathrm{d}\nu_2 \, \mathrm{d}k \cdots \mathrm{e}^{\mathrm{i}k|\boldsymbol{x}'-\boldsymbol{x}|\cos\nu_1}. \tag{E.7}$$

We carry out the ν_1 integration asymptotically by integrating by parts. The result is

$$\int k^2 \sin\nu_1 \, \mathrm{d}\nu_1 \, \mathrm{d}\nu_2 \, \mathrm{d}k \cdots \mathrm{e}^{\mathrm{i}k|\boldsymbol{x}'-\boldsymbol{x}|\cos\nu_1} = \frac{1}{|\boldsymbol{x}'-\boldsymbol{x}|} \int \mathrm{i}k \, \mathrm{d}\nu_2 \, \mathrm{d}k \cdots [\mathrm{e}^{-\mathrm{i}k|\boldsymbol{x}'-\boldsymbol{x}|} - \mathrm{e}^{\mathrm{i}k|\boldsymbol{x}'-\boldsymbol{x}|}]. \tag{E.8}$$

In this evaluation between limits, the rest of the integrand has to be evaluated at the endpoints in ν_1, namely, 0 and π. These pick the same direction of $\hat{\boldsymbol{k}}$, so the integrand is the same in both limits. Furthermore, the integrand now becomes independent of the second angle ν_2 and that integration merely produces a factor of 2π. Consequently,

$$\int k^2 \sin\nu_1 \, \mathrm{d}\nu_1 \, \mathrm{d}\nu_2 \, \mathrm{d}k \cdots \mathrm{e}^{\mathrm{i}k|\boldsymbol{x}'-\boldsymbol{x}|\cos\nu_1} = \frac{2\pi}{|\boldsymbol{x}'-\boldsymbol{x}|} \int_0^\infty \mathrm{i}k \, \mathrm{d}k \cdots [\mathrm{e}^{-\mathrm{i}k|\boldsymbol{x}'-\boldsymbol{x}|} - \mathrm{e}^{\mathrm{i}k|\boldsymbol{x}'-\boldsymbol{x}|}]. \tag{E.9}$$

The integrand denoted by $\cdots$ in this result is independent of k. Thus, this is a distributional integral. To evaluate it, first replace k by $-k$ in the second term here to obtain

$$\begin{aligned} \int k^2 \sin\nu_1 \, \mathrm{d}\nu_1 \, \mathrm{d}\nu_2 \, \mathrm{d}k \cdots \mathrm{e}^{\mathrm{i}k|\boldsymbol{x}'-\boldsymbol{x}|\cos\nu_1} &= \frac{2\pi}{|\boldsymbol{x}'-\boldsymbol{x}|} \int_{-\infty}^\infty \mathrm{i}k \, \mathrm{d}k \cdots \mathrm{e}^{-\mathrm{i}k|\boldsymbol{x}'-\boldsymbol{x}|} \\ &= -\cdots \frac{4\pi^2}{|\boldsymbol{x}'-\boldsymbol{x}|} \delta'(|\boldsymbol{x}'-\boldsymbol{x}|). \end{aligned} \tag{E.10}$$

We need an interpretation of the distribution $-\delta'(r)/r$ that is consistent with the fact that this analysis is being carried out in three-dimensional spherical polar coordinates. To determine that interpretation, we observe that in polar coordinates

$$\begin{aligned} -\int f(r) \frac{\delta'(r)}{r} \, \mathrm{d}V &= -\int f(r) \frac{\delta'(r)}{r} r^2 \, \mathrm{d}r \sin\nu_1 \, \mathrm{d}\nu_1 \, \mathrm{d}\nu_2 = -\int f(r) r \delta'(r) \, \mathrm{d}r \sin\nu_1 \, \mathrm{d}\nu_1 \, \mathrm{d}\nu_2 \\ &= 4\pi \int_0^\infty f(r) \delta(r) \, \mathrm{d}r = 2\pi f(0). \end{aligned}$$

Here, we take a half-weight of the delta-function appearing at an endpoint of integration; this is the natural value in polar coordinates. From this result, we conclude that

$$-\frac{\delta'(|\boldsymbol{x}'-\boldsymbol{x}|)}{|\boldsymbol{x}'-\boldsymbol{x}|} = 2\pi\delta(\boldsymbol{x}'-\boldsymbol{x}). \tag{E.11}$$

We use this distributional identity in the distributional equality (E.10) to complete the asymptotic integration in $\boldsymbol{k}$. The resulting delta-function allows us to carry out the integrations in $\boldsymbol{x}'$ in the norm representation (E.5) and leads to the result (28) for an asymptotic estimate of the norm $\|(K^\dagger K)^{-1}\|$.

Appendix F. An identity for the Beylkin determinant

Here, we derive the result equation (31), expressing the Beylkin determinant in terms of the WKBJ amplitude. We start from the definition of the Beylkin determinant implicit in equation (E.4). Note that the three rows of the matrix whose determinant is to be calculated are merely the gradient of the travel time and its derivatives with respect to the coordinates that describe the source/receiver array. Let us rewrite that gradient as a product of its magnitude and unit direction vector:

$$\nabla_x \tau(\boldsymbol{x}, \boldsymbol{\xi}) = \frac{2\cos\theta}{v(\boldsymbol{x})}\hat{\boldsymbol{\nu}}. \tag{F.1}$$

The magnitude stated here is derived in Bleistein *et al* (2001), equation (5.1.45). When we differentiate this product, there is one term that is proportional to $\hat{\boldsymbol{\nu}}$ and one that is not. In calculating the determinant, we can neglect the portion of the second and third rows that are proportional to $\hat{\boldsymbol{\nu}}$, because they are in the same direction as the entire first row. Therefore,

$$h(\boldsymbol{x}, \boldsymbol{\xi}) = \det\begin{bmatrix} \dfrac{2\cos\theta}{v(\boldsymbol{x})}\hat{\boldsymbol{\nu}} \\ \dfrac{2\cos\theta}{v(\boldsymbol{x})}\dfrac{\partial\hat{\boldsymbol{\nu}}}{\partial\xi_1} \\ \dfrac{2\cos\theta}{v(\boldsymbol{x})}\dfrac{\partial\hat{\boldsymbol{\nu}}}{\partial\xi_2} \end{bmatrix} = \left[\frac{2\cos\theta}{v(\boldsymbol{x})}\right]^3 \det\begin{bmatrix} \hat{\boldsymbol{\nu}} \\ \dfrac{\partial\hat{\boldsymbol{\nu}}}{\partial\xi_1} \\ \dfrac{\partial\hat{\boldsymbol{\nu}}}{\partial\xi_2} \end{bmatrix}. \tag{F.2}$$

Since $\hat{\boldsymbol{\nu}}$ is a unit vector, its derivatives with respect to ξ_1 and ξ_2 are both orthogonal to the vector $\hat{\boldsymbol{\nu}}$. Thus, if we think of this determinant as a triple scalar product, the cross product of the last two rows is colinear with $\hat{\boldsymbol{\nu}}$ and we can write

$$h(\boldsymbol{x}, \boldsymbol{\xi}) = \left[\frac{2\cos\theta}{v(\boldsymbol{x})}\right]^3 \left|\frac{\partial\hat{\boldsymbol{\nu}}}{\partial\xi_1} \times \frac{\partial\hat{\boldsymbol{\nu}}}{\partial\xi_2}\right|. \tag{F.3}$$

Hence, within a sign we obtain the result (27) for the Beylkin determinant divided by the magnitude of the gradient of travel time. Since we require the absolute value for the Jacobian of coordinate transformation, the sign ambiguity is of no consequence.

We can also see from this last expression for the Beylkin determinant in equation (F.3) where the difficulty arises in computing the Beylkin determinant when (ξ_1, ξ_2) are parameters on the acquisition surface. The connection via rays, especially for the case of common-offset data, is particularly difficult to compute. On the other hand, when the integration parameters that we use are the spherical polar coordinates of $\boldsymbol{k}$ at the image point, the cross product appearing in equation (F.3) is just $\sin\nu_1$. If we were to use cylindrical coordinates for $\hat{\boldsymbol{\nu}}$, then the cross product is just equal to 1!

Equation (F.3) is the most concise representation of the Beylkin determinant in 3D.

References

Bleistein N 2003 A proposal for full waveform Kirchhoff inversion *Internal Research Report* Veritas DGC Inc.

Bleistein N, Cohen J K and Stockwell J W 2001 *Mathematics of Multidimensional Seismic Imaging, Migration and Inversion* (New York: Springer)

Bleistein N and Gray S H 2002 A proposal for common-opening-angle migration/inversion *Center for Wave Phenomena Research Report* CWP-420

Burridge R, de Hoop M V, Miller D and Spencer C 1998 Multiparameter inversion in anisotropic media *Geophys. J. Int.* **134** 757–77

Chapman C 1985 Ray theory andits extensions: WKBJ and Maslov seismogram *J. Geophys.* **58** 27–43

Claerbout J F 1970 Coarse grid calculations of waves in inhomogeneous media with application to delineation of complicated seismic structure *Geophysics* **35** 407–18

Claerbout J F 1971 Toward a unified theory of reflector imaging *Geophysics* **36** 467–81

Claerbout J F 1985 *Imaging the Earth's Interior* (Oxford: Blackwell)

Hanitzsch C 1997 Comparision of weights in prestack amplitude-preserving Kirchhoff depth migration *Geophysics* **62** 1812–6

Keho T H and Beydoun W B 1988 Paraxial ray Kirchhoff migration *Geophysics* **53** 1540–6

Kravtsov Y and Orlov Y 1993 *Caustics, Catastrophes and Wavefields* (Berlin: Springer)

Hertweck T, Jäger C, Goertz A and Schleicher J 2003 Aperture effects in 2.5D Kirchhoff migration: A geometrical explanation *Geophysics* **68** 1673–84

Xu S, Chauris H, Lambaré G and Noble M S 2001 Common-angle migration: A strategy for imaging complex media *Geophysics* **66** 1877–94

Zhang Y, Zhang G and Bleistein N 2003 True amplitude wave equation migration arising from true-amplitude one-way wave equations *Inverse Problems* **19** 1113–38

Zhang Y, Zhang G and Bleistein N 2004a Theory of true amplitude one-way wave equations and true amplitude common-shot migration *Geophysics* **70** E1–E10

Zhang Y, Xu S, Zhang G and Bleistein N 2004b How to obtain true-amplitude common-angle gathers from one-way wave equation migration *74th Ann. Mtg Soc. Expl. Geophys.* Expanded Abstracts, Migration 3.7